J. Fluid Mech. (1998), *vol.* 376, *pp.* 319–350. Printed in the United Kingdom

© 1998 Cambridge University Press

Elementary stratified flows with instability at large Richardson number

By ANDREW J. MAJDA AND MICHAEL G. SHEFTER

Courant Institute of Mathematical Sciences, New York University, New York 10012, USA

(Received 6 March 1998 and in revised form 3 August 1998)

In contrast to the Miles–Howard theorem for inviscid steady shear flow in stably stratified fluids, explicit elementary time-periodic solutions of the Boussinesq equations are developed here which are unstable for arbitrarily large Richardson numbers. These elementary flows are parameterized through solutions of a nonlinear pendulum equation and involve spatially constant but temporally varying vorticity and density gradients which interact through advection and baroclinic vorticity production. Exact nonlinear solutions for arbitrary wave-like disturbances for these flows are developed here and Floquet theory combined with elementary numerical calculations is utilized to demonstrate instability at all large Richardson numbers. The dominant inviscid instability for these non-parallel flows is a purely two-dimensional parametric instability with twice the period of the elementary flow and persists for all Reynolds numbers and the wide range of Prandtl numbers, $1 \leqslant Pr \leqslant 200$, investigated here. Similar elementary time-periodic solutions of the Boussinesq equations in a constant external strain field are developed here which reduce to uniform shear flows in one extreme limit and the time-periodic vortical flows in the other extreme limit. These flows are stable in a strict sense for large Richardson numbers; however there is transient large-amplitude non-normal behaviour which yields effective instability for a wide range of Richardson numbers. For example, suitable initial perturbations can amplify by at least a factor of fifty with exponential growth for short times for $\mathscr{R}i = 1, |\sigma| \leqslant 0.5$ and $\mathscr{R}i = 5, |\sigma| \leqslant 0.1$, with σ the amplitude of the external strain.

1. Introduction

One of the basic analytical results for stably stratified fluid flows is the celebrated Miles–Howard theorem (Miles 1961; Howard 1961). This theorem states that steady shear flows $\boldsymbol{V} = (v(z), 0, 0)$ in an inviscid stably stratified fluid are linearly stable for all Richardson numbers, Ri, satisfying

$$Ri > \tfrac{1}{4}, \quad Ri = \frac{\mathscr{N}^2}{\left(\partial v/\partial z\right)^2} \tag{1.1}$$

with $\mathscr{N}^2 = -g(\partial\rho/\partial z)/\rho_b$, the square of the buoyancy or Brunt–Väisälä frequency. This criterion for stability is often interpreted and applied literally for time-dependent flow fields in numerical modelling for the atmosphere or ocean. For example, a popular turbulent eddy diffusivity used in numerical simulations in the atmosphere/ocean community is the Lilly–Smagorinsky eddy diffusivity (Smagorinsky 1963; Lilly 1967) where the turbulent eddy diffusivity is completely switched off and set to zero for $Ri \geqslant \overline{Ri} \geqslant \frac{1}{4}$ with $\overline{Ri}$ of order unity. Recent use of this turbulent diffusivity in

https://doi.org/10.1017/S0022112098003085 Published online by Cambridge University Press

atmospheric science can be found in Bretherton *et al.* (1998) and several of the references cited there; work by Siegel & Domaradzki (1994) and Lavelle & Smith (1996) as well as numerous references in those papers, are recent examples of the use of such eddy diffusivity in computations for physical oceanography.

With all of the above background, an obvious interesting question is the following one: Are there time-dependent stably stratified flows which are unstable for Richardson numbers larger than $\frac{1}{4}$? The main goal of this paper is to build explicit elementary time-dependent and non-parallel stably stratified flows which are unambiguously unstable for all (arbitrarily large) Richardson numbers. The existence of such examples contrasts strongly with the Miles–Howard theorem for steady shear flows and provides a strong warning signal for interpreting the Miles–Howard theorem indiscriminately for time-dependent stably stratified flows. Earlier important work by Drazin (1977) establishes that propagating unidirectional gravity waves are unstable for large local Richardson numbers.

The elementary solutions of the stably stratified Boussinesq equations which are unstable for all Richardson numbers are given by certain time-periodic flows with spatially constant but temporally varying vorticity and density gradients (see § 2.3 below). These elementary exact solutions have the form

$$\left.\begin{aligned} &\rho = \rho_b + \sin\theta(t)x - \cos\theta(t)z, \\ &\boldsymbol{v} = \begin{pmatrix} \frac{1}{2}\omega(t)z \\ 0 \\ -\frac{1}{2}\omega(t)x \end{pmatrix}, \end{aligned}\right\} \tag{1.2}$$

written in the appropriate non-dimensional coordinates, where $\theta(t)$ represents the angle between the density gradient and the (negative vertical) z-axis while the velocity field is a time-varying vortex with axis along the y-direction. The strength of the vortex $\omega(t)$ and the magnitude of the density gradient interact through advection and baroclinic vorticity production (see §2.3 below) and define an exact solution of the Boussinesq equations provided that $\omega(t)$ and $\theta(t)$ satisfy

$$\left.\begin{aligned} &\frac{\omega(t)}{2} = -\frac{\mathrm{d}\theta}{\mathrm{d}t}, \\ &\frac{\mathrm{d}^2\theta}{\mathrm{d}t^2} = -\sin\theta(t). \end{aligned}\right\} \tag{1.3}$$

Thus, the exact solutions (1.2) are defined through the nonlinear pendulum equations (1.3). With the preliminary results from § 2.3, we establish the linear and nonlinear instability of these time-periodic flows in § 4 through analysis and elementary numerical integration based on Floquet theory which is summarized in § 3.

We establish that these flows from (1.2) and (1.3) are unstable at all Richardson numbers and that the dominant mode of instability is purely two-dimensional with motion in the (x, z)-plane; furthermore, the modes of dominant linearized instability involve parametric instability with a period of growth which is twice the period of the underlying fluid flow defined in (1.2) and (1.3). Also, these flows remain unstable even with finite viscosity and heat conduction effects with the same basic structure of dominant instability as for the inviscid case for all Reynolds numbers and for all Prandtl numbers investigated here, i.e. Pr, with $1 \leqslant Pr \leqslant 200$. We remark that the exact solutions (1.2) and (1.3) admit the following interpretation: Deflect the horizontal isopycnal surface by an arbitrarily small initial angle, θ_0, with $|\theta_0| \ll 1$

https://doi.org/10.1017/S0022112098003085 Published online by Cambridge University Press

and with $\mathrm{d}\theta/\mathrm{d}t|_{t=0} = 0$. Then, the stably stratified fluid responds through baroclinic vorticity production with time-periodic motions generating a small-amplitude vortex defined by $\omega(t)$ through (1.2) and (1.3) and never deflects the isopycnal surface beyond the small angle, $|\theta_0|$. Such flows have no overturning as discussed in § 2.3 yet are unstable for arbitrarily small deflection angles through parametric two-dimensional instability, even with finite viscosity and heat conduction. Of course the growth rate of the instability decreases with increasing Richardson number.

How general beyond these flows given by (1.2) and (1.3) are fluid flows exhibiting instability at Richardson numbers larger than $\frac{1}{4}$? In §2.4 we introduce basic large-scale solutions of the Boussinesq equations with velocity given by

$$\boldsymbol{v} = \begin{pmatrix} \frac{1}{2}(\omega(t)+\sigma)z \\ 0 \\ \frac{1}{2}(-\omega(t)+\sigma) \end{pmatrix} \tag{1.4}$$

and corresponding spatially constant density gradient, $\boldsymbol{b}(t) = (b_1(t), 0, b_3(t))^T$. The constant value, σ, corresponds to an imposed large-scale strain flow. For the initial value, $\omega(0) = \sigma$, these elementary solutions are steady shear flows while for $\sigma = 0$, we recover the basic time-dependent flows (1.2) and (1.3); thus, the elementary flows with the structure (1.4) range between the two extreme cases of stability and instability at large Richardson numbers discussed earlier. In § 2.4, we construct elementary time-periodic solutions of the Boussinesq equations with the velocity field having the form (1.4) with $\sigma \neq 0$.

In § 5, we study the linear and nonlinear stability of such solutions. In a strict sense, we find stability of these flows for all large Richardson numbers in the sense that wave-like perturbations eventually decay at large times. However, there is transient large-amplitude non-normal behaviour (Farrell & Ioannou 1993) which can yield effective instability for a wide range of Richardson numbers when this growth is coupled with the inherent nonlinearity in the system. For example, suitable initial perturbations amplify by at least a factor of fifty with exponential growth for short times for

$$\left.\begin{aligned} \mathscr{R}i = 1 \text{ and } |\sigma| \leqslant 0.5, \\ \mathscr{R}i = 5 \text{ and } |\sigma| \leqslant 0.1, \\ \mathscr{R}i = 10 \text{ and } |\sigma| \leqslant 0.05. \end{aligned}\right\} \tag{1.5}$$

In all of our discussion above, we have utilized the most conservative choice of Richardson number, $\mathscr{R}i$, for time-dependent flows with this number always smaller than the classical Richardson number; this Richardson number is discussed in detail in §2.2.

The main technical ingredient for our linear and nonlinear stability analysis is a straightforward generalization for the stratified Boussinesq equations of an important construction due to Craik & Criminale (1986) of exact solutions of the homogeneous Navier–Stokes equations involving large-scale flows with spatially constant gradients. For the Boussinesq equations, the exact solution procedure for the large-scale flow is summarized in § 2.1 while the equations for the superimposed wave-like disturbances are presented in § 3. For the readers' convenience, a detailed derivation of these equations for Boussinesq solutions is presented in the Appendix of this paper. Over the last few years, the basic technique utilized here has been very fruitful in discussing

https://doi.org/10.1017/S0022112098003085 Published online by Cambridge University Press

instability for homogeneous incompressible flows (Craik 1989; Craik & Allen 1992; Lifschitz & Hameiri 1991). Uses of Floquet theory as well as suitable generalizations for stability theory for homogeneous incompressible flows have been developed in this context (Bayly 1986; Bayly, Holm & Lifschitz 1996; Forster & Craik 1996).

2. A family of elementary stratified flows

In this paper we investigate some stability properties of simple stratified flows, satisfying the non-rotating Boussinesq equations

$$\left.\begin{aligned} \frac{\mathrm{D}\boldsymbol{v}}{\mathrm{D}t} &= -\nabla p - \frac{g}{\rho_b}\rho \boldsymbol{e}_3 + \nu\Delta\boldsymbol{v}, \\ \operatorname{div}\boldsymbol{v} &= 0, \\ \frac{\mathrm{D}\tilde{\rho}}{\mathrm{D}t} &= \kappa\Delta\tilde{\rho}, \end{aligned}\right\} \tag{2.1}$$

where $\boldsymbol{v}$ is the flow velocity, ρ is the total density, p is the hydrodynamic pressure, ρ_b is the constant reference fluid density, $\boldsymbol{e}_3$ is the unit vertical coordinate vector, ν is the kinematic viscosity, and κ is the heat conductivity. The total density ρ is given as the sum of the ambient density ρ_b and the perturbation density $\tilde{\rho}$. Below we use the notation (x, y, z) or (x_1, x_2, x_3) for the spatial coordinates when either is more convenient in a particular discussion.

A simple but meaningful framework for this study is provided by a special family of exact solutions to (2.1). These solutions consist of a large-scale piece, which has a linear structure in space (but evolving in time) together with small-scale nonlinear plane wave perturbations. In this section we will focus our attention on the large-scale part. In §§ 3, 4 and 5 we will study the small-scale perturbations to these solutions. Consider special spatially linear solutions of (2.1), with the form

$$\left.\begin{aligned} \boldsymbol{v}(\boldsymbol{x}, t) &= \mathscr{D}(t)\boldsymbol{x} + \tfrac{1}{2}\boldsymbol{\omega}(t)\times\boldsymbol{x}, \\ \tilde{\rho}(\boldsymbol{x}, t) &= \rho_b + \boldsymbol{b}(t)\cdot\boldsymbol{x}, \\ p(\boldsymbol{x}, t) &= \tfrac{1}{2}\hat{\boldsymbol{P}}(t)\boldsymbol{x}\cdot\boldsymbol{x}, \end{aligned}\right\} \tag{2.2}$$

where $\mathscr{D}(t)$ is an arbitrary 3×3 symmetric traceless strain matrix and $\boldsymbol{\omega}(t) = \operatorname{curl}\boldsymbol{v}$ is the vorticity, which is a function of time alone. The vorticity $\boldsymbol{\omega}(t)$ has an equivalent representation by a skew-symmetric matrix $\Omega(t)$,

$$\Omega(t)\boldsymbol{h} = \tfrac{1}{2}\boldsymbol{\omega}(t)\times\boldsymbol{h}, \quad \text{for any vector } \boldsymbol{h}. \tag{2.3}$$

It follows from (2.2), that the vorticity $\boldsymbol{\omega}(t)$ and the density gradient $\boldsymbol{b}(t)$ replace the original variables $\boldsymbol{v}$ and ρ in the description of the flow field. In order to satisfy the Boussinesq equations, the functions $\boldsymbol{\omega}(t)$ and $\boldsymbol{b}(t)$ must satisfy the following equations:

$$\left.\begin{aligned} \frac{\mathrm{d}\boldsymbol{\omega}(t)}{\mathrm{d}t} &= \mathscr{D}(t)\boldsymbol{\omega}(t) + \frac{g}{\rho_b}\begin{pmatrix} -b_2(t) \\ b_1(t) \\ 0 \end{pmatrix}, \\ \frac{\mathrm{d}\boldsymbol{b}}{\mathrm{d}t} &= -\mathscr{D}(t)\boldsymbol{b}(t) + \tfrac{1}{2}\boldsymbol{\omega}(t)\times\boldsymbol{b}(t). \end{aligned}\right\} \tag{2.4}$$

The details of the derivation of these equations are presented in the Appendix. Pressure plays the role of a Lagrange multiplier and is determined entirely by the

https://doi.org/10.1017/S0022112098003085 Published online by Cambridge University Press

incompressibility condition from $\mathscr{D}, \boldsymbol{\omega}, \boldsymbol{b}$ by

$$-\hat{\boldsymbol{P}} = \frac{\mathrm{d}\mathscr{D}}{\mathrm{d}t} + \mathscr{D}(t)^2 + \Omega(t)^2 + \frac{g}{2\rho_b}(\boldsymbol{e}_3 \otimes \boldsymbol{b} + \boldsymbol{b} \otimes \boldsymbol{e}_3), \tag{2.5}$$

where $\otimes$ is the usual tensor product of two vectors.

All elementary solutions with the form in (2.2) formally have velocity and density which become unbounded for large values of $|\boldsymbol{x}|$; these elementary flows should be considered as local Taylor approximations of more general stratified flow fields. For homogeneous fluid flow, this point of view has been justified by formal WKB techniques (Lifschitz & Hameiri 1991).

2.1. *Basic large-scale flows*

In this paper we consider special large-scale flows generated by (2.2) and (2.4) which involve a single vortex located at the origin with $\boldsymbol{\omega}(t)$ always perpendicular to the (x_1, x_3)-plane, and distorted by a strain flow slanted at the 45° angle:

$$\left.\begin{aligned} \boldsymbol{\omega}(t) = \omega(t)\boldsymbol{e}_2, \quad \boldsymbol{b}(t) = \begin{pmatrix} b_1(t) \\ 0 \\ b_3(t) \end{pmatrix}, \\ \boldsymbol{v} = \begin{pmatrix} 0 & \frac{1}{2}(\omega(t)+\sigma) \\ \frac{1}{2}(-\omega(t)+\sigma) & 0 \end{pmatrix} \begin{pmatrix} x_1 \\ x_3 \end{pmatrix}. \end{aligned}\right\} \tag{2.6}$$

The parameter σ in (2.6) is associated with the strength of the strain flow (jet). Important special solutions of (2.6) are the set of equilibrium points $\omega(t) = \sigma$. It is easy to see that the corresponding flows are simple vertical shears of the horizontal velocity v_1 in the (x_1, x_3)-plane.

To close the formulation, we must select some reasonable initial conditions for (2.6). An appropriate set is given by initially stable vertical stratification and some initial strength of the vortex,

$$\omega(0) = \omega_0, \quad b_1(0) = 0, \quad b_3(0) = -B_0, \quad B_0 > 0. \tag{2.7}$$

To non-dimensionalize the problem, we select the ambient density ρ_b, initial vertical density gradient B_0, and g to set the scales. Then, the variables in equations (2.6) and (2.7) take the following non-dimensional form:

$$\boldsymbol{x} \to \frac{\rho_b}{B_0}\tilde{\boldsymbol{x}}, \quad t \to \frac{\tilde{t}}{\mathscr{N}}, \quad b \to B_0\tilde{b}, \quad \omega \to \mathscr{N}\tilde{\omega}, \quad \sigma \to \mathscr{N}\tilde{\sigma}, \quad \boldsymbol{v} \to \frac{\mathscr{N}\rho_b}{B_0}\tilde{\boldsymbol{v}},$$

in terms of the four non-dimensional numbers

$$\mathscr{N}^2 = \frac{gB_0}{\rho_b}, \quad Fr = \frac{\omega_0}{\mathscr{N}}, \quad Re = \frac{\rho_b^2\omega_0}{\nu B_0^2}, \quad Pr = \frac{\nu}{\kappa}. \tag{2.8}$$

Here, $\mathscr{N}$ is the Brunt–Väisälä buoyancy frequency, Fr is the Froude number, Re is the Reynolds number and Pr is the Prandtl number associated with this flow. It is worthwhile mentioning that the Reynolds number involves a time scale determined by the strength of the original vortex and a length scale determined by the large-scale density variations.

In the remainder of this paper, non-dimensional variables replace dimensional ones with all primes dropped. The Boussinesq equations assume the following non-

https://doi.org/10.1017/S0022112098003085 Published online by Cambridge University Press

dimensional form:

$$\left.\begin{aligned} \frac{\mathrm{D}\boldsymbol{v}}{\mathrm{D}t} &= -\nabla p - \rho \boldsymbol{e}_3 + Fr\,Re^{-1}\Delta \boldsymbol{v}, \\ \operatorname{div} \boldsymbol{v} &= 0, \\ \frac{\mathrm{D}\tilde{\rho}}{\mathrm{D}t} &= Fr\,Re^{-1}Pr^{-1}\Delta\tilde{\rho}. \end{aligned}\right\} \tag{2.9}$$

The non-dimensional form of the system (2.4) in the form (2.6) and initial conditions (2.7) is given by

$$\left.\begin{aligned} \dot{\omega} &= b_1, \\ \dot{b}_1 &= \tfrac{1}{2}(-\sigma + \omega)b_3, \\ \dot{b}_3 &= -\tfrac{1}{2}(\sigma + \omega)b_1, \end{aligned}\right\} \tag{2.10}$$

$$\omega(0) = Fr\,; \quad b_1(0) = 0; \quad b_3(0) = -1. \tag{2.11}$$

2.2. *The Richardson number for time-dependent flows*

In this paper, we study how the stability properties of stratified non-stationary flows depend on the Richardson number. First of all, we need to properly define a Richardson number for the elementary time-dependent flows in § 2.1. In the stationary case, the Richardson number measures the square of the ratio of time scales associated with shearing motion and buoyancy. The natural scale for the buoyancy time is given in units inversely proportional to the time-dependent effective Brunt–Väisälä frequency

$$N^2(t) = -\frac{g}{\rho_b}\frac{\partial\tilde{\rho}(x,z,t)}{\partial z}. \tag{2.12}$$

It is not so straightforward, however, to select a scale associated with the shearing time. It is possible to suggest two competing definitions for a dynamic Richardson number given by

$$Ri_1(t) = \frac{N^2(t)}{\left(\partial \boldsymbol{v}_H/\partial z\right)^2}, \quad Ri_2(t) = \frac{N^2(t)}{|\nabla \times \boldsymbol{v}|^2 + \operatorname{tr}\mathscr{D}^2}. \tag{2.13}$$

The Richardson number Ri_1, is the standard one used for time-independent shear flows while $Ri_2(t)$ generalizes this quantity naturally to flows with varying vorticity and strain. We note that Ri_2 satisfies $Ri_2 < Ri_1$, so that this is a more conservative choice for deciding instability in time dependent flows. We utilize the generalized Richardson number $Ri_2(t)$ in all of our discussion below and denote this quantity by $Ri(t)$. In order to compare different time-dependent flows, we will need to select some 'typical' value of the Richardson number. It is quite natural to select the overall minimum of the function, $\mathscr{R}i = \min Ri(t)$, as the most conservative choice for stability studies of time-dependent flows. This is exactly what we do in this paper.

https://doi.org/10.1017/S0022112098003085 Published online by Cambridge University Press

2.3. *A vortex in stably stratified flow*

As a first example of the large-scale flows (2.6) we consider a single vortex with no external strain field, that is, $\sigma = 0$, so that

$$\left.\begin{aligned} \boldsymbol{\omega}(t) = \omega(t)\boldsymbol{e}_2; \quad \boldsymbol{b}(t) = \begin{pmatrix} b_1(t) \\ 0 \\ b_3(t) \end{pmatrix}; \\ \boldsymbol{v} = \begin{pmatrix} 0 & \frac{1}{2}\omega(t) \\ -\frac{1}{2}\omega(t) & 0 \end{pmatrix} \begin{pmatrix} x_1 \\ x_3 \end{pmatrix}. \end{aligned}\right\} \tag{2.14}$$

In this example, the fluid is engaged in circular motion about the origin, caused by a single vortex with intensity changing in time due to baroclinic vorticity production. The equations of motion in this case simplify to

$$\left.\begin{aligned} \frac{\mathrm{d}\omega}{\mathrm{d}t} = b_1, \\ \frac{\mathrm{d}}{\mathrm{d}t}\begin{pmatrix} b_1 \\ b_3 \end{pmatrix} = \begin{pmatrix} 0 & \frac{1}{2}\omega(t) \\ -\frac{1}{2}\omega(t) & 0 \end{pmatrix} \begin{pmatrix} b_1 \\ b_3 \end{pmatrix}, \end{aligned}\right\} \tag{2.15}$$

with the same initial conditions (2.11) as before. Since the matrix describing the evolution of $\boldsymbol{b}$ is skew-symmetric, the length of the vector $\boldsymbol{b}$ remains constant. Therefore we can introduce the phase variable $\theta(t)$, so that

$$\begin{pmatrix} b_1 \\ b_3 \end{pmatrix} = \begin{pmatrix} \sin\theta(t) \\ -\cos\theta(t) \end{pmatrix}. \tag{2.16}$$

Using the first equation of (2.15), we reinterpret the last two equations in (2.15) as describing the evolution of the phase,

$$\frac{\mathrm{d}\theta}{\mathrm{d}t} = -\omega(t)/2, \quad \frac{\mathrm{d}\omega}{\mathrm{d}t} = \sin\theta(t). \tag{2.17}$$

Taking one more derivative, we reduce this system to the pendulum equation

$$2\frac{\mathrm{d}^2\theta}{\mathrm{d}t^2} = -\sin\theta(t) \tag{2.18}$$

with conserved energy given by the Hamiltonian

$$\mathscr{H} = \dot{\theta}^2 - \cos\theta. \tag{2.19}$$

The first question in the context of stability analysis for these elementary vortex motions is how the overturning of the fluid is related to the pendulum dynamics and the Richardson number. Clearly, overturning occurs when b_3 becomes negative. For the 'pendulum' motion, it can happen, according to (2.16), for

$$\cos\theta(t) < 0. \tag{2.20}$$

Only strong enough oscillations can cause overturning of the initially stably stratified fluid, and the initial strength of vorticity ω_0 determines the amplitude of oscillations. One easily finds from the first equation in (2.17) and the conservation of energy (2.19)

https://doi.org/10.1017/S0022112098003085 Published online by Cambridge University Press

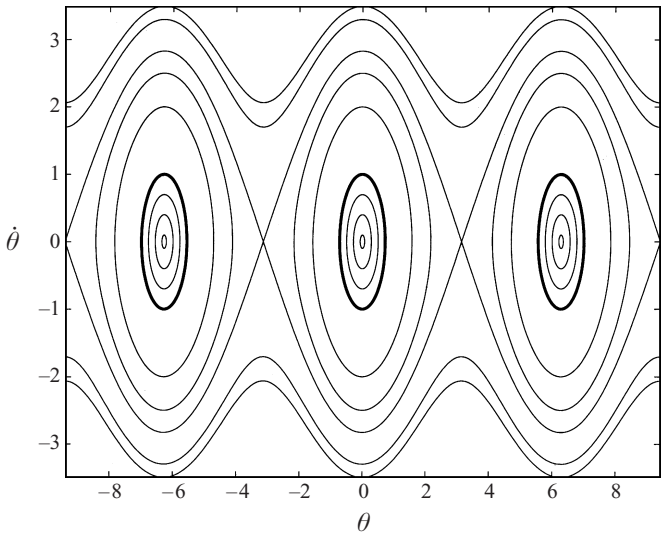


FIGURE 1. Elementary vortical flows represented on the phase portrait of a simple pendulum. Bold contours, $\mathscr{H}_0 = 0$, separate the flows without overturning (located inside the contours) for $\mathscr{R}i > \frac{1}{4}$ and with overturning (located outside the contours) for $\mathscr{R}i < \frac{1}{4}$.

that the overturning criterion (2.20) can take place only when

$$|\dot\theta(0)| = 2\left|\frac{\omega_0}{\mathscr{N}}\right| > 1. \tag{2.21}$$

We are now ready to relate this criterion for overturning to the dynamic Richardson number, $\mathscr{R}i$, introduced in §2.2. The time-dependent Brunt–Väisälä frequency, $N(t)$, has a simple sinusoidal form and the vorticity ω can be obtained from the first equation of (2.17) and the conservation of energy (2.19), so that the Richardson number is equal to

$$Ri(t) = \frac{N^2(t)}{|\nabla \times \boldsymbol{v}|^2} = \frac{\cos\theta(t)}{4(\mathscr{H}_0 + \cos\theta(t))}. \tag{2.22}$$

The pendulum energy, $\mathscr{H}_0$, is conserved during oscillations and is entirely determined by the initial vorticity via $\mathscr{H}_0 = \dot\theta^2(0) - 1$ and (2.17). It is easy to see from (2.22) that the Richardson number attains its minimum at time $t = 0$,

$$\mathscr{R}i = Ri(0) = \frac{N^2(0)}{\omega_0^2} = \frac{\mathscr{N}^2}{\omega_0^2} \leqslant Ri(t), \tag{2.23}$$

while the phase $\theta(t)$ varies between $\theta_{min} = -\arccos\left(1 - 1/(4\mathscr{R}i)\right)$ and $\theta_{max} = \arccos\left(1 - 1/(4\mathscr{R}i)\right)$, according to (2.19). It is easy now to formulate the overturning condition (2.21) in terms of the Richardson number $\mathscr{R}i$:

$$\left.\begin{array}{l}\text{flows with } \mathscr{R}i > \frac{1}{4} \text{ never overturn; the energy } \mathscr{H}_0 \text{ takes negative values;}\\ \text{all flows with } \mathscr{R}i < \frac{1}{4} \text{ do overturn; the energy } \mathscr{H}_0 \text{ takes positive values.}\end{array}\right\} \tag{2.24}$$

The last observation brings our choice of Richardson number for these flows to be analogous with the famous $\frac{1}{4}$ result of Miles (1961) and Howard (1961).

https://doi.org/10.1017/S0022112098003085 Published online by Cambridge University Press

The phase portrait described by (2.17) is shown in figure 1. To find the period for each closed orbit, it is sufficient to integrate (2.19) by quadrature

$$T = 4\int_0^{\theta_s} \frac{\mathrm{d}\theta}{(\cos(\theta)-\cos(\theta_s))^{1/2}}, \tag{2.25}$$

where θ_s is the maximum deflection of the pendulum.

2.4. *A vortex in a strain flow*

A more general example of elementary solutions is provided by adding a 45° rotated strain field in the (x_1, x_3)-plane to the single vortex flow described in the previous section. Equations (2.10) have an integral of motion

$$b_3 + \tfrac{1}{2}\sigma\omega + \tfrac{1}{4}\omega^2 = -1 + \tfrac{1}{2}\sigma Fr + \tfrac{1}{4}Fr^2. \tag{2.26}$$

Using this integral, we reduce the size of the system by one, eliminating b_3, so that the reduced system becomes

$$\left.\begin{aligned} \dot{\omega} &= b_1, \\ \dot{b}_1 &= \tfrac{1}{2}(-\sigma+\omega)\left(\mathscr{C} - \frac{\sigma}{2}\omega - \frac{\omega^2}{4}\right), \end{aligned}\right\} \tag{2.27}$$

with $\mathscr{C}$ determined by the initial conditions,

$$\omega(0) = Fr\,; \quad b_1(0) = 0; \quad \mathscr{C} = -1 + \frac{\sigma Fr}{2} + \frac{Fr^2}{4}. \tag{2.28}$$

Solutions to (2.27) are closed trajectories in the (ω, b_1)-plane. In contrast to the vortex flows (2.14), the trajectories can cross now, being just projections of full three-dimensional phase-space trajectories, since the parameter $\mathscr{C}$ depends on the initial conditions. Hamiltonian structure on its own is not crucial for this problem. However, it is quite important for the stability analysis to be able to compute the period of solutions to (2.27). The period can be computed with the help of a conserved Hamiltonian $\mathscr{H}_{Fr;\sigma}$ for (2.27), which can be introduced in the following way:

$$\mathscr{H}_{Fr;\sigma}(\omega, b_1) = \frac{b_1^2}{2} + V(\omega), \tag{2.29}$$

$$V(\omega) = \frac{\omega^4}{32} + \frac{\sigma\omega^3}{24} - \frac{1}{4}\left(\mathscr{C}(\sigma, Fr) + \frac{\sigma^2}{2}\right)\omega^2 + \frac{\sigma\mathscr{C}(\sigma, Fr)}{2}\omega. \tag{2.30}$$

This Hamiltonian arises because the 2×2 system (2.27) describes the motion of a particle in a quartic potential inside a well bounded by the two roots of $V(\omega)-V(Fr) = 0$ straddling the 'centre' $\omega = \sigma$. For each initial value of the vorticity, Fr, the shape of the potential and location of the roots is different, reflecting the dependence of $\mathscr{C}$ on the initial conditions. The equilibrium states

$$\omega = \sigma, \quad b_1 = 0, \quad b_3 = -1, \tag{2.31}$$

correspond to simple vertical shears of the horizontal velocity v_1.

The period of motion along trajectories in the (ω, b_1)-plane can be found in terms of elliptic integrals (Tabor 1989). If we represent function $V(\omega)-V(Fr)$ as the following product:

$$V(\omega) - V(Fr) = \tfrac{1}{32}(\omega - r_1)(\omega - r_2)(\omega - r_3)(\omega - r_4), \tag{2.32}$$

https://doi.org/10.1017/S0022112098003085 Published online by Cambridge University Press

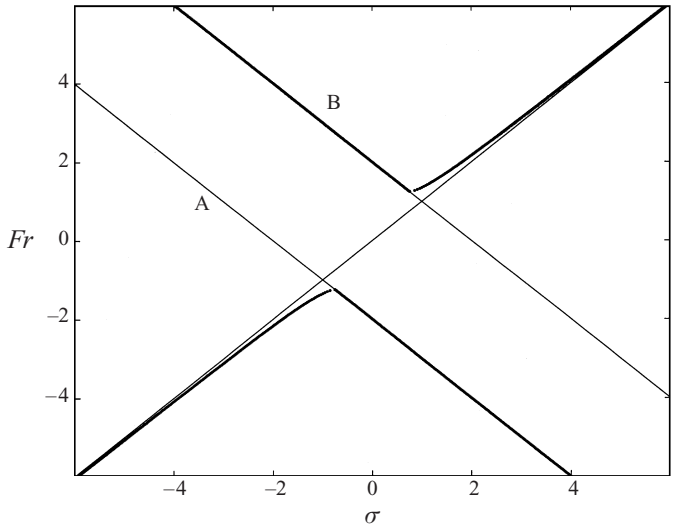


FIGURE 2. Elementary flows with and without overturning, parameterized by the Froude number, Fr, and the strain parameter σ. The region between the top bold curve and the bottom bold curve has no overturning. Lines A and B coincide with parts of the bottom and the top bold curves respectively. The line $Fr = \sigma$ corresponds to simple shears.

and note that for $|\sigma| < 1$ only two of the roots (r_1 and r_2) are real, with the other two a complex conjugate pair, then we can express the period of motion in terms of the following constants:

$$\left.\begin{aligned} &R_1 = ((r_1 - r_3)(r_1 - r_4))^{1/2}\,; \quad R_2 = ((r_2 - r_3)(r_2 - r_4))^{1/2}\,, \\ &\kappa^2 = \frac{(r_1 - r_2)^2 - (R_1 - R_2)^2}{4R_1R_2}\,; \quad \Omega = \pm\left(\frac{R_1R_2}{32}\right)^{1/2}, \\ &K(\kappa) = \int_0^{\pi/2} (1 - \kappa^2 \sin^2\xi)^{-1/2} \mathrm{d}\xi\,; \quad T = \frac{4K(\kappa)}{|\Omega|}. \end{aligned}\right\} \tag{2.33}$$

We have numerically investigated the occurrence of overturning in these elementary solutions as a function of the strain parameter σ. The regions where elementary solutions described by (2.27) and (2.28) present overturning and the boundaries separating these regions from the stably stratified solutions are shown in figure 2.

The transition from stably stratified flow for all times to flows with overturning occurs along the bold curves in this figure. It is easy to show that the left part of the top curve and the right part of the bottom curve coincide with straight lines B and A, with equations $Fr + \sigma = \pm 2$. For further insight, we present a plot of the Richardson number $Ri(t)$ evolution (figure 3) for a stable solution located in the (Fr, σ)-plane near the boundary of the region where solutions overturn (shown in figure 2). The figure clearly shows that the graph of $Ri(t)$ has slope zero where $Ri(t) = 0$. This observation along with the definition of Richardson number given in (2.13) suggests that the vertical component of the density gradient $b_3(t)$ of borderline solutions vanishes together with its first derivative,

$$b_3(t^*) = 0, \quad \frac{\mathrm{d}b_3}{\mathrm{d}t}(t^*) = 0. \tag{2.34}$$

https://doi.org/10.1017/S0022112098003085 Published online by Cambridge University Press

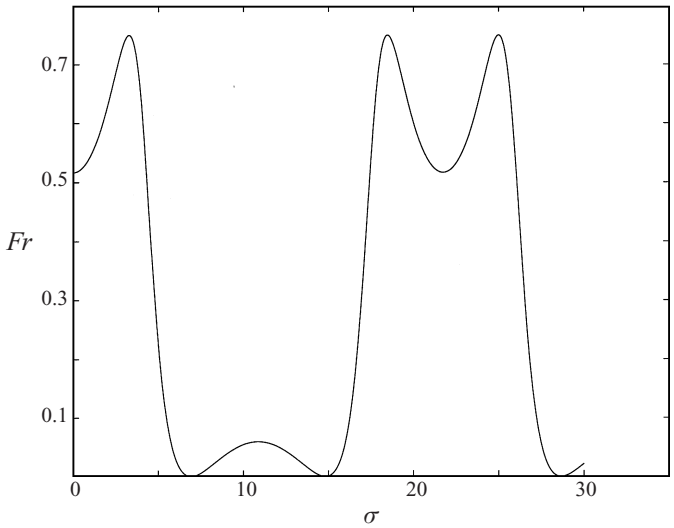


FIGURE 3. Evolution of a typical dynamic Richardson number $Ri_2(t)$ for an elementary solution near the boundary of the region without overturning in the (Fr, σ)-plane at $\sigma = 0.7$, $Fr = -2.7$.

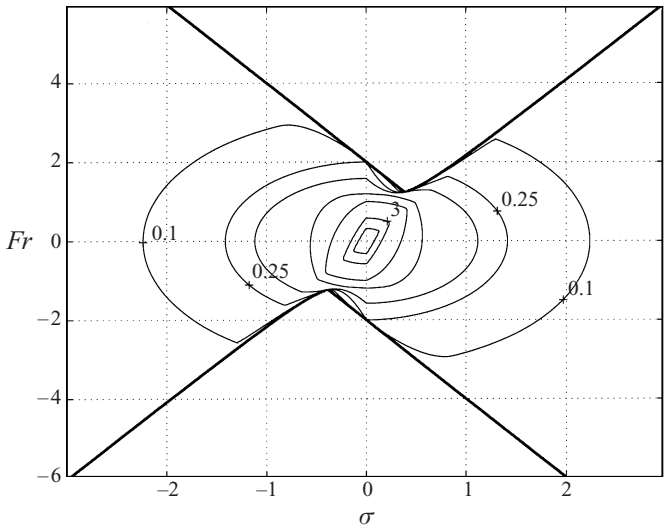


FIGURE 4. Level curves of the minimum Richardson number $\mathscr{R}i$ for elementary flows. The nested contours, $\mathscr{R}i = 0.1, 0.25, 3$ are labelled.

It follows then from (2.26) that

$$b_3(t) = -1 + \frac{\sigma Fr}{2} + \frac{Fr^2}{4} - \frac{\sigma}{2}\omega(t) - \frac{\omega^2(t)}{4} = 0. \tag{2.35}$$

After elimination of ω from (2.34) we get

$$(Fr + \sigma)^2 = 4, \tag{2.36}$$

which is the equation for lines A and B.

To complete the discussion, we present figure 4, which shows the level lines of

https://doi.org/10.1017/S0022112098003085 Published online by Cambridge University Press

the Richardson number $\mathscr{R}i$, defined as the absolute minimum of $Ri(t)$, given by the second formula of (2.13).

In conclusion, we would like to mention that the exact solutions described in this section satisfy the Boussinesq equations (2.1) either with or without viscosity and heat conduction, since they have a linear spatial structure.

3. Exact nonlinear stability analysis

In the previous section we studied in detail the construction of elementary exact solutions to the nonlinear Boussinesq equations without rotation. We have also introduced a global Richardson number for such flows and generalized it for the time-dependent case. Finally, we tied this Richardson number to considerations regarding overturning of the density profile. In this section we introduce a second family of exact solutions for (2.1), in addition to the one discussed above. Solutions of the second family are in the form of nonlinear plane waves. Remarkably, as developed in the Appendix, the quasi-linear approximation is exact for the superposition of two solutions of this type (Craik & Criminale 1986). This property allows us to treat plane wave solutions as nonlinear perturbations of the elementary flows described in § 2. Even though the elementary flows remain stably stratified, they can be (and often are) unstable to these small-scale perturbations. Stability analysis, therefore, becomes extremely important, providing clear examples of the relationship between overturning and the dynamic Richardson number in these flows.

To fix the ideas, we introduce the following family of plane wave perturbations:

$$\left.\begin{aligned} \boldsymbol{v}^*(\boldsymbol{x},t) &= \boldsymbol{A}(t)F(\boldsymbol{\alpha}(t)\cdot\boldsymbol{x}),\\ \tilde{\rho}^*(\boldsymbol{x},t) &= B(t)F(\boldsymbol{\alpha}(t)\cdot\boldsymbol{x}),\\ p^*(\boldsymbol{x},t) &= P(t)G(\boldsymbol{\alpha}(t)\cdot\boldsymbol{x}), \end{aligned}\right\} \tag{3.1}$$

where $\boldsymbol{\alpha}$ is the wave vector, associated with a plane wave, $\boldsymbol{A}(t), B(t)$ and $P(t)$ are the nonlinear perturbation velocity, density and pressure amplitudes respectively. The functions $F(s)$ and $G(s)$ define the shape of the plane wave; they are always related to each other in a simple way: $G'(s) = F(s)$. Solutions defined by the superposition of (2.2) and (3.1) have the form

$$\left.\begin{aligned} \boldsymbol{v}(\boldsymbol{x},t) &= \boldsymbol{v}_l + \boldsymbol{v}^* = \mathscr{D}(t)\boldsymbol{x} + \tfrac{1}{2}\boldsymbol{\omega}(t)\times\boldsymbol{x} + \boldsymbol{A}(t)F(\boldsymbol{\alpha}(t)\cdot\boldsymbol{x}),\\ \tilde{\rho}(\boldsymbol{x},t) &= \tilde{\rho}_l + \tilde{\rho}^* = \rho_b + \boldsymbol{b}\cdot\boldsymbol{x} + B(t)F(\boldsymbol{\alpha}(t)\cdot\boldsymbol{x}),\\ p(\boldsymbol{x},t) &= p_l + p^* = \tfrac{1}{2}\hat{\boldsymbol{P}}(t)\boldsymbol{x}\cdot\boldsymbol{x} + P(t)G(\boldsymbol{\alpha}(t)\cdot\boldsymbol{x}), \end{aligned}\right\} \tag{3.2}$$

and satisfy the Boussinesq equations as long as, in addition to (2.4), the following equations hold:

$$\left.\begin{aligned} \frac{\mathrm{d}\boldsymbol{\alpha}}{\mathrm{d}t} &= -\boldsymbol{V}^T(t)\boldsymbol{\alpha}(t),\\ \frac{\mathrm{d}\boldsymbol{A}}{\mathrm{d}t} &= -\boldsymbol{V}(t)\boldsymbol{A}(t) + \boldsymbol{\alpha}\frac{2(\boldsymbol{V}^T(t)\boldsymbol{\alpha}(t)\cdot\boldsymbol{A}(t))}{|\boldsymbol{\alpha}|^2} + \frac{g}{\rho_b}\left[\frac{\alpha_3}{|\boldsymbol{\alpha}|^2}\boldsymbol{\alpha} - \boldsymbol{e}_3\right]B(t) - \nu k^2|\boldsymbol{\alpha}|^2\boldsymbol{A},\\ \frac{\mathrm{d}B}{\mathrm{d}t} &= -\boldsymbol{A}(t)\cdot\boldsymbol{b}(t) - \kappa k^2|\boldsymbol{\alpha}|^2 B. \end{aligned}\right\} \tag{3.3}$$

See the Appendix for a detailed derivation of these equations, where it is also shown that only sinusoidal waves with $F(s) = \sin(ks + \phi_0)$ satisfy the Boussinesq equations

https://doi.org/10.1017/S0022112098003085 Published online by Cambridge University Press

(2.1) with non-zero viscosity and heat conduction, while an arbitrary wave profile $F(s)$ is possible when these diffusive terms vanish.

Next, we non-dimensionalize (3.3) in a fashion consistent with the non-dimensionalization of the elementary flows (2.8) from § 2. To set the scales, we again utilize the ambient density ρ_b, the initial value of the vertical density gradient B_0, and g. With this choice, the non-dimensional variables are

$$\boldsymbol{\alpha} \to \frac{B_0}{\rho_b}\tilde{\boldsymbol{\alpha}}, \quad \boldsymbol{A} \to \left(\frac{g\rho_b}{B_0}\right)^{1/2} \tilde{\boldsymbol{A}}, \quad B \to \rho_b \tilde{B}.$$

Since only non-dimensional variables will be used throughout the rest of the paper, we will drop the tildes. Equations (3.3) take the following non-dimensional form:

$$\left.\begin{aligned} \frac{\mathrm{d}\boldsymbol{\alpha}}{\mathrm{d}t} &= -\boldsymbol{V}^T(t)\boldsymbol{\alpha}(t), \\ \frac{\mathrm{d}\boldsymbol{A}}{\mathrm{d}t} &= -\boldsymbol{V}(t)\boldsymbol{A}(t) + \boldsymbol{\alpha}\frac{2(\boldsymbol{V}^T(t)\boldsymbol{\alpha}(t)\cdot\boldsymbol{A}(t))}{|\boldsymbol{\alpha}|^2} + \left[\frac{\alpha_3}{|\boldsymbol{\alpha}|^2}\boldsymbol{\alpha} - \boldsymbol{e}_3\right] B(t) - Fr\,Re^{-1}k^2|\boldsymbol{\alpha}|^2\boldsymbol{A}, \\ \frac{\mathrm{d}B}{\mathrm{d}t} &= -\boldsymbol{A}(t)\cdot\boldsymbol{b}(t) - Fr\,Re^{-1}Pr^{-1}k^2|\boldsymbol{\alpha}|^2 B. \end{aligned}\right\} \quad (3.4)$$

We will discuss now in some detail the methods we will use to investigate the stability of the elementary solutions from § 2 to the nonlinear perturbations in (3.1).

3.1. *Some background facts*

The functions $\boldsymbol{\omega}$ and $\boldsymbol{b}$, defining the elementary solutions (2.2) are periodic functions of time in all examples considered in this paper, with the period computed according to either (2.25) or (2.33). We will show in § 4 that for all flows generated by a single vortex with $\sigma = 0$ in (2.15), the time evolution of a perturbation wave vector $\boldsymbol{\alpha}$ can be expressed in terms of a large-scale phase θ (introduced in (2.16)) in a very simple form, being a periodic function of time itself. It is easy to see that the system (3.4) then becomes linear in $\boldsymbol{A}$ and B with coefficients periodic in time. We will use Floquet theory, designed especially for such equations to study the stability of perturbations. Here we list several facts useful for the stability analysis (Hochstadt 1975).

Fundamental matrix. For any non-autonomous linear system of ordinary differential equations $\mathrm{d}\boldsymbol{x}/\mathrm{d}t = \mathscr{A}(t)\boldsymbol{x}$ one can define a fundamental matrix $\mathscr{R}(t)$ which solves

$$\mathscr{R}' = \mathscr{A}(t)\mathscr{R}, \quad \mathscr{R}(0) = \boldsymbol{I}. \quad (3.5)$$

Then any solution of a general initial value problem

$$\boldsymbol{x}' = \mathscr{A}(t)\boldsymbol{x}, \quad \boldsymbol{x}(0) = \boldsymbol{x}_0 \quad (3.6)$$

can be written as $\boldsymbol{x}(t) = \mathscr{R}(t)\boldsymbol{x}_0$.

Liouville's Theorem states that for any flow, described by a linear system with time-dependent coefficients, the determinant of the fundamental matrix can be expressed in terms of trace of the system matrix,

$$\det \mathscr{R}(t) = \exp \int_0^t \mathrm{tr}\ \mathscr{A}(s)\,\mathrm{d}s. \quad (3.7)$$

In §§ 4.1 and 4.2 the matrix $\mathscr{A}(t)$ is 3×3 with coefficients periodic in time and zero trace. Liouville's theorem applied to such matrices implies that $\det\mathscr{R}(T) = 1$.

https://doi.org/10.1017/S0022112098003085 Published online by Cambridge University Press

Periodicity. Floquet theory says that for any T-periodic matrix $\mathscr{A}(t)$ there exists matrix $\mathscr{P}(t)$ and constant matrix $\mathscr{F}$ such that

$$\mathscr{R}(t) = \mathscr{P}(t)\mathrm{e}^{\mathscr{F}t}, \quad \mathscr{P}(t+T) = \mathscr{P}(t). \tag{3.8}$$

Since $\mathscr{P}(t+T) = \mathscr{P}(t)$ and $\mathscr{R}(T) = \mathscr{P}(T)\mathrm{e}^{\mathscr{F}T} = \mathrm{e}^{\mathscr{F}T}$ it suffices to show that all eigenvalues of $\mathrm{e}^{\mathscr{F}T}$ are not greater than 1 to prove stability and to find an eigenvalue larger than one to have instability.

Ertel's Theorem and eigenvalues. In this part we will show, using Ertel's theorem about conservation of potential vorticity, that one of the eigenvalues of the fundamental matrix $\mathscr{R}(t)$ used in our construction is equal to 1. Note that for the particular type of flow introduced in (3.2), potential vorticity assumes the following form:

$$\begin{aligned} q &= (\boldsymbol{\omega}_{total}(\boldsymbol{x},t)\cdot\nabla\rho(\boldsymbol{x},t)) = ((0,\omega,0)+(\boldsymbol{\alpha}\times\boldsymbol{A})F')\cdot((b_1,0,b_3)+BF'\boldsymbol{\alpha}) \\ &= \alpha_2\omega B + (\boldsymbol{\alpha}\times\boldsymbol{A})\cdot(b_1,0,b_3), \end{aligned} \tag{3.9}$$

where $\cdot$ stands for the usual scalar product of two vectors. Ertel's theorem states that potential vorticity, q, computed in the formula written above must be time invariant. Note that q is a linear function of the amplitude functions $\boldsymbol{A}(t)$ and $B(t)$ from (3.2), with the coefficients depending on the mean flow parameters $\omega(t), b_1(t), b_3(t)$ and also $\boldsymbol{\alpha}(t)$. These parameters do not depend on $\boldsymbol{A}(t)$ and $B(t)$ and can be shown to be periodic in time (it easily follows from the Hamiltonian structure of (2.27) and from (4.2) below). In all cases considered in this paper, $A_2(t)$ decouples from the system (3.3). Therefore, it suffices to consider a 3×3 system for the functions $A_1(t), A_3(t)$ and $B(t)$ alone, with the appropriate 3×3 fundamental matrix $\mathscr{R}(t)$. To conclude, we can write Ertel's theorem for an arbitrary solution $(A_1(t), A_3(t), B(t)) = \mathscr{R}(t)\boldsymbol{x}_0$, with an arbitrary initial condition $\boldsymbol{x}_0$, as

$$(\boldsymbol{e}(t)\cdot\mathscr{R}(t)\boldsymbol{x}_0) = \eta, \tag{3.10}$$

where $\boldsymbol{e}(t)$ is a certain T-periodic vector function and $\mathscr{R}(0) = \boldsymbol{I}$. It follows then that

$$\begin{aligned} (\boldsymbol{e}(0)\cdot\boldsymbol{x}_0) &= (\boldsymbol{e}(0)\cdot\mathscr{R}(0)\boldsymbol{x}_0) = q(0) \equiv q(T) = (\boldsymbol{e}(T)\cdot\mathscr{R}(T)\boldsymbol{x}_0) \\ &= (\boldsymbol{e}(0)\cdot\mathscr{R}(T)\boldsymbol{x}_0) = (\mathscr{R}^T(T)\boldsymbol{e}(0)\cdot\boldsymbol{x}_0). \end{aligned} \tag{3.11}$$

Since the last formula is valid for any $\boldsymbol{x}_0$ we deduce that $\mathscr{R}^T(T)\boldsymbol{e}(0) = \boldsymbol{e}(0)$; therefore, $\mathscr{R}^T(T)$ has the eigenvalue 1 in its spectrum, with $\boldsymbol{e}(0)$ as a corresponding eigenvector. Thus, for the two other eigenvalues λ_1, λ_2, we have

$$\begin{aligned} 1+\lambda_1+\lambda_2 &= \operatorname{tr}\mathscr{R}(T), \\ \lambda_1\lambda_2 &= \det\mathscr{R}(T) = 1, \end{aligned}$$

which yields the following expression for the eigenvalues:

$$\lambda_{1,2} = \frac{\operatorname{tr}\mathscr{R}(T) - 1 \pm \left((1-\operatorname{tr}\mathscr{R}(T))^2 - 4\right)^{1/2}}{2}. \tag{3.12}$$

The last formula implies that the eigenvalues form a complex conjugate pair when the discriminant is negative. This case corresponds to stability. In order to get instability, the discriminant must be positive, i.e.

$$|\operatorname{tr}\mathscr{R}(T) - 1| > 2. \tag{3.13}$$

In the borderline case $|\operatorname{tr}\mathscr{R}(T) - 1| = 2$ the predictions of Floquet theory (neutral stability) need to be checked by a separate consideration.

https://doi.org/10.1017/S0022112098003085 Published online by Cambridge University Press

Numerical evaluation of a singular integral. In the next sections, we integrate (3.4) to determine stability or instability according to the above criterion. This note deals with computation of the period of periodic solutions to (2.15) using formula (2.25). This formula provides an exact answer; however, it is not appropriate for practical computations, since the integrand becomes singular near the right-hand limit of integration $\theta = \theta_s$. In order to bypass this problem, we propose to separate the singular and regular parts of the integral:

$$\int_0^{\theta_s} \frac{\mathrm{d}\theta}{(\cos(\theta)-\cos(\theta_s))^{1/2}} = \int_0^{\theta_s-\delta} \frac{\mathrm{d}\theta}{(\cos(\theta)-\cos(\theta_s))^{1/2}} + \int_{\theta_s-\delta}^{\theta_s} \frac{\mathrm{d}\theta}{(\cos(\theta)-\cos(\theta_s))^{1/2}}.$$

The first of the two integrals on the right-hand side can be computed with any of the standard integrating procedures (e.g. trapezoidal rule with Romberg extrapolation or Simpson rule). For the singular integral we propose to use the power series expansion

$$\begin{aligned}\int_{\theta_s-\delta}^{\theta_s} \frac{\mathrm{d}\xi}{((\cos(\theta_s-\xi)-\cos(\theta_s)))^{1/2}} &= \int_0^{\delta} \frac{\mathrm{d}\xi}{(\cos(\theta_s-\xi)-\cos(\theta_s))^{1/2}} \\ &= \frac{1}{(\sin(\theta_s))^{1/2}} \left\{ 2\,\delta^{1/2} + \tfrac{1}{6}\delta^{3/2}\cot(\theta_s) + \tfrac{1}{5}\delta^{5/2}\left(\tfrac{1}{6} + \tfrac{3}{16}\cot^2(\theta_s)\right)\right. \\ &\quad + \tfrac{1}{7}\delta^{7/2}\left(\tfrac{1}{12}\cot(\theta_s) + \tfrac{5}{64}\cot^3(\theta_s)\right) \\ &\quad \left. + \tfrac{1}{9}\delta^{9/2}\left(\tfrac{1}{80} + \tfrac{3}{64}\cot^2(\theta_s) + \tfrac{35}{1024}\cot^4(\theta_s)\right)\right\} + O(\delta^{11/2}).\end{aligned}$$

This formula can be extended to include higher powers in δ, if greater accuracy is desired. The threshold value δ separating regular and singular parts of the integral is determined experimentally to ensure fastest convergence.

For direct numerical simulations of (3.4) we have used the fourth-order Kapp–Rentrop method for stiff differential equations (Press *et al.* 1992) with adaptive time step and replaced it with fourth-order Runge–Kutta when (3.4) did not present stiff behaviour.

4. Instability at large Richardson numbers

In this section we discuss how stability properties of certain non-stationary flows depend on the Richardson number. In many time-dependent problems it is implicitly assumed that stability occurs at Richardson numbers bigger than $\frac{1}{4}$. Here we present simple but very instructive examples involving the simple vortex flows in stable stratification described earlier in § 2.3, where such a criterion does not work and, in fact, instability occurs for arbitrarily large Richardson numbers. We explicitly show the unstable modes and discuss the type of instability observed. We also study the influence of viscosity and heat conduction on these stability properties.

The simple vortex with stable stratification

We numerically investigate the stability of large scale stably stratified flows generated by the simple vortex in (2.14). Recall that we established in § 2.3 that these flows cause no overturning, provided the Richardson number is greater than the 'classical' value of $\frac{1}{4}$. We investigate the behaviour of the nonlinear plane wave perturbations in (3.1) for these solutions. This study reveals that appropriate amplitudes of the perturbations introduced by (3.1) yield growing modes for any arbitrarily large Richardson number. First, we discuss inviscid flows with no heat conduction and show that all wavelengths are subject to instability. In the second situation, we discuss instability with viscosity

https://doi.org/10.1017/S0022112098003085 Published online by Cambridge University Press

and heat conduction added and show that the influence of Reynolds and Prandtl numbers only limits the bandwidth of wave vectors that carry unstable perturbations. In both cases these flows always have exponentially growing oscillations with twice the period of the underlying vortex motion. Such growth is the typical signature of a parametric instability.

4.1. *Inviscid instability*

For the simple vortex flows (2.14)–(2.25) from § 2.3 the equations for perturbation variables $\boldsymbol{\alpha}, \boldsymbol{A}$ and B in (3.4) take the following form:

$$\left.\begin{aligned}
&\dot{\alpha}_1 = \tfrac{1}{2}\omega(t)\alpha_3, \quad \dot{\alpha}_2 = 0, \quad \dot{\alpha}_3 = -\tfrac{1}{2}\omega(t)\alpha_1,\\
&\dot{A}_1 = -\tfrac{1}{2}\omega(t)A_3 + \frac{2}{|\alpha|^2}\left(-\frac{\omega(t)}{2}\alpha_3 A_1 + \frac{\omega(t)}{2}\alpha_1 A_3\right)\alpha_1 + \frac{\alpha_3\alpha_1}{|\alpha|^2}B,\\
&\dot{A}_2 = \frac{2}{|\alpha|^2}\left(-\frac{\omega(t)}{2}\alpha_3 A_1 + \frac{\omega(t)}{2}\alpha_1 A_3\right)\alpha_2 + \frac{\alpha_3\alpha_2}{|\alpha|^2}B,\\
&\dot{A}_3 = \tfrac{1}{2}\omega(t)A_1 + \frac{2}{|\alpha|^2}\left(-\frac{\omega(t)}{2}\alpha_3 A_1 + \frac{\omega(t)}{2}\alpha_1 A_3\right)\alpha_3 + \left(\frac{\alpha_3^2}{|\alpha|^2} - 1\right)B,\\
&\dot{B} = -b_1 A_1 - b_3 A_3.
\end{aligned}\right\} \tag{4.1}$$

The first three equations of (4.1) are independent of the rest and have the following general solution:

$$\boldsymbol{\alpha}(t) = \alpha_0 \begin{pmatrix} \sin(\phi)\sin(\theta(t)+\theta_0) \\ \cos(\phi) \\ -\sin(\phi)\cos(\theta(t)+\theta_0) \end{pmatrix}, \quad \alpha_0, \theta_0 \text{ and } \phi \text{ arbitrary constants}, \tag{4.2}$$

where $\theta(t)$ is the phase variable defined in (2.16). Next, we notice that the equations for the perturbation amplitudes $\boldsymbol{A}, B$ include only homogeneous terms in $\boldsymbol{\alpha}$. Thus, the length $|\boldsymbol{\alpha}|^2$ of the wave vector can be set equal to unity without any loss of generality. It is clear from (4.1) that the equation for A_2 decouples and can be integrated independently after A_1, A_3 and B have been determined. In view of these remarks, the system in (4.1) reduces to

$$\begin{pmatrix} \dot{A}_1 \\ \dot{A}_3 \\ \dot{B} \end{pmatrix} = \begin{pmatrix} -\omega\alpha_1\alpha_3 & (\alpha_1^2 - \frac{1}{2})\omega & \alpha_1\alpha_3 \\ (\alpha_3^2 - \frac{1}{2})\omega & \omega\alpha_1\alpha_3 & \alpha_1\alpha_3 \\ -b_1 & -b_3 & 0 \end{pmatrix} \begin{pmatrix} A_1 \\ A_3 \\ B \end{pmatrix}, \tag{4.3}$$

where the large-scale solution ω, b_1, b_3 is known from the solution of the pendulum equation (2.18) via (2.16) and (2.17). From (4.2) with $\alpha_0 = 1$, the perturbation wave vector $\boldsymbol{\alpha}$ has unit length and depends on the phase $\theta(t)$, with two arbitrary angular parameters θ_0 and ϕ. The angle ϕ determines the deviation of the perturbation wave from the (x_1, x_3)-plane (that of unperturbed motion), while θ_0 defines the initial position of the wave vector in the (x_1, x_3)-plane. The system of equations (4.3) for A_1, A_3, B is linear with coefficients periodic in time, which depend on the known functions ω, b_1, b_3 as well as on the parameters ϕ and θ_0 and is perfectly suited for the Floquet theory discussed in §3.1.

To make the analysis easier, we notice that the linear system in (4.3) is traceless. This implies that the product of all three eigenvalues of the fundamental matrix is equal to unity. We showed in § 3.1 that conservation of potential vorticity implies that one of the eigenvalues is equal to 1. Therefore, the stability check can be reduced to the verification of just a single number, the fundamental matrix trace. According

https://doi.org/10.1017/S0022112098003085 Published online by Cambridge University Press

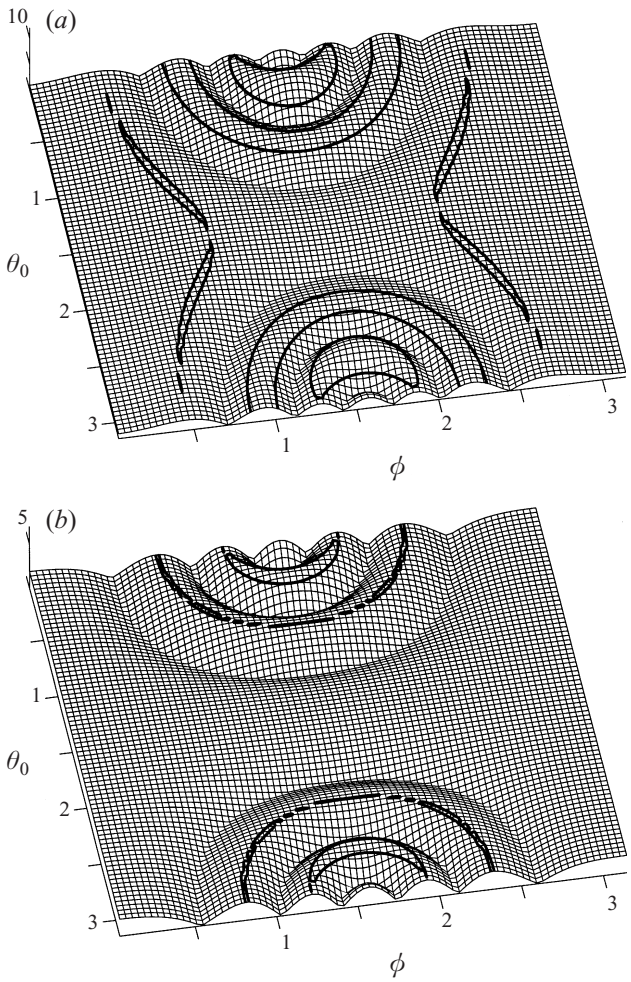


FIGURE 5. Fundamental matrix trace, $\mathrm{tr}\,\mathscr{R}(t)$, as a function of initial orientation of the perturbation wave vector for the vortical elementary flow with Richardson number $\mathscr{R}i = 1$ in (*a*) and $\mathscr{R}i = 7$ in (*b*). The contour lines separate regions of stability (with $\mathrm{tr}\,\mathscr{R} < 2$) from regions of instability (with $\mathrm{tr}\,\mathscr{R} > 2$).

to the criterion in (3.13), when this trace is greater than 2, plane wave perturbations cause instability of the basic motion, while a trace smaller than 2 corresponds to stable perturbations. One can compute the growth rates, once the fundamental matrix trace is known, according to the following formula from (3.12):

$$\lambda = \frac{\mathrm{tr}\,\mathscr{R}(T) - 1 \pm \left((1 - \mathrm{tr}\,\mathscr{R}(T))^2 - 4\right)^{1/2}}{2}, \tag{4.4}$$

where $\mathscr{R}$ denotes the fundamental matrix.

Figure 5 presents the stability regions in parameter space (θ_0, ϕ) for two different values of Richardson number, $\mathscr{R}i = 1$ and $\mathscr{R}i = 7$. The regions with trace bigger than 2 on this diagram correspond to unstable plane wave perturbations of vortex motions. Clearly, the most prominent instabilities are located along the $\phi = \pi/2$ lines on these diagrams. According to (4.2), perturbations with $\phi = \pi/2$ are purely two-dimensional in the (x_1, x_3)-plane.

https://doi.org/10.1017/S0022112098003085 Published online by Cambridge University Press

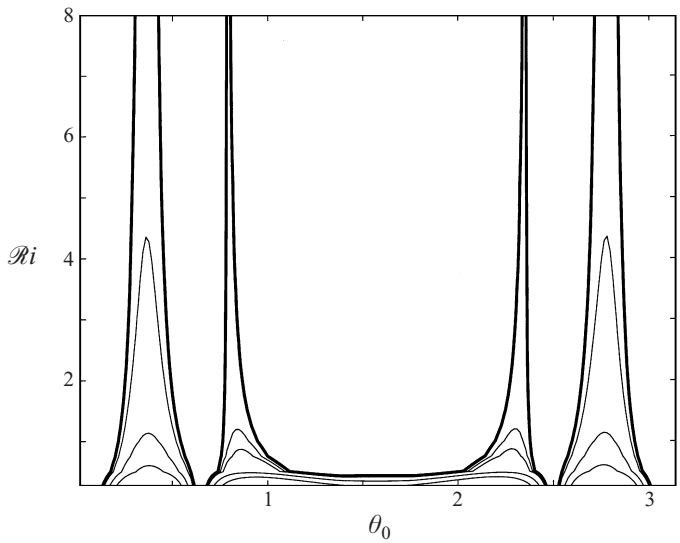


FIGURE 6. Regions of instability, as the Richardson number varies, with fundamental matrix trace larger than 2, for two-dimensional perturbations in the (x_1, x_3)-plane. The coordinate axes are θ_0 and $\mathscr{R}i$, respectively.

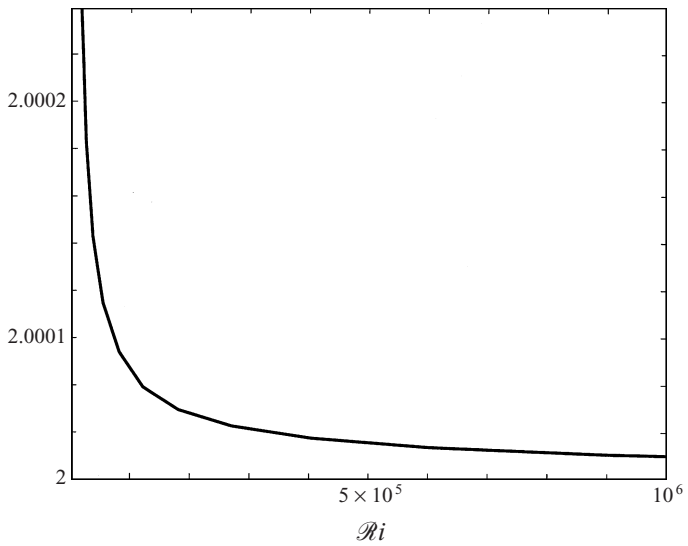


FIGURE 7. Maximum fundamental matrix trace for large values of the Richardson number $\mathscr{R}i$.

Since instabilities presented by the two-dimensional perturbations are the strongest, we study them separately. Figure 6 shows regions of instability for two-dimensional perturbations of single vortex flows with Richardson numbers varying from $\frac{1}{4}$ to 8. Although unstable parts in the θ_0-direction shrink at larger Richardson numbers, they never disappear. In fact, we were able to check this statement for huge values of $\mathscr{R}i$. In figure 7 we plot the fundamental matrix trace for (4.3) versus Richardson number reaching very large values of order 10^6. As before, $\mathrm{tr}\,\mathscr{R} > 2$

https://doi.org/10.1017/S0022112098003085 Published online by Cambridge University Press

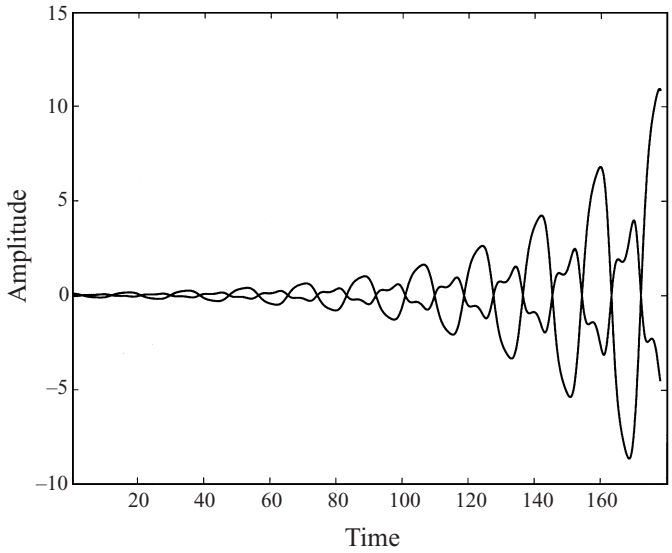


FIGURE 8. Amplitudes of the horizontal velocity perturbation undergo exponential growth in time via parametric instability.

is the instability condition. Even though the growth rates become extremely small at these large Richardson numbers, nevertheless there is unambiguous evidence for instability.

To conclude our discussion, we comment on the physical nature of the instabilities discussed above. As a typical case, we chose a two-dimensional perturbation of a single vortex with $\mathscr{R}i = 20$. Figure 8 shows the time evolution of the amplitudes of the two-dimensional perturbation velocities A_1 and A_3. The perturbation is two-dimensional, with θ_0 picked at its most unstable value (at the middle of the instability strip located near $\theta_0 = 2.75$ in figure 6), while the initial conditions were taken along the unstable eigenmode of (4.3). Figure 8 clearly presents exponentially growing oscillations. Five growing oscillations occur during ten oscillations of the underlying basic 'pendulum' flow and such behaviour is a typical signature of parametric instability. The visualization of the flow field (omitted here for brevity) suggests that local overturning will develop from the instabilities in the basic flow, even with $\mathscr{R}i = 20$. Of course, we expect that the fully nonlinear evolution of perturbations of the complete plane wave solutions in (3.2) is subject itself to nonlinear instability, so figure 8 has to be interpreted as demonstrating only linear instability of the basic state. Examples of such nonlinear instability can be found in Lombard & Riley (1996).

4.2. *Instability with viscosity and heat conduction*

As we have mentioned before, the elementary exact solutions described in § 2 are insensitive to the terms associated with viscosity and heat conduction. Therefore, we can use the same single vortex solutions (2.14) as the basic motion. The equations for perturbations amplitudes, however, are modified in the presence of Reynolds and Prandtl numbers, as described in (3.4). The wave profiles are restricted to the sinusoidal form $F(y) = \sin(ky + \phi_0)$ and several extra terms have to be included in

https://doi.org/10.1017/S0022112098003085 Published online by Cambridge University Press

the equations

$$\left.\begin{aligned}
\dot{A}_1 &= -\tfrac{1}{2}\omega A_3 + \frac{\alpha_1}{\alpha_0^2}(-\omega\alpha_3 A_1 + \omega\alpha_1 A_3) + \frac{\alpha_3\alpha_1}{\alpha_0^2}B - Fr\,Re^{-1}k^2\alpha_0^2 A_1,\\
\dot{A}_3 &= \tfrac{1}{2}\omega A_1 + \frac{\alpha_3}{\alpha_0^2}(-\omega\alpha_3 A_1 + \omega\alpha_1 A_3) + \left(\frac{\alpha_3^2}{\alpha_0^2} - 1\right)B - Fr\,Re^{-1}k^2\alpha_0^2 A_3,\\
\dot{B} &= -b_1 A_1 - b_3 A_3 - Fr\,Pr^{-1}Re^{-1}k^2\alpha_0^2 B,
\end{aligned}\right\} \tag{4.5}$$

where k is the wavenumber. Expressions (4.2) can be used for the wave vector $\boldsymbol{\alpha}$. Now we cannot simply dismiss the wave vector length, α_0, as irrelevant, as we did in the inviscid case of § 4.1. However, certain reduction in the number of independent parameters is also possible for (4.5).

Clearly, the wave vector length α_0 is not an independent parameter. It enters (4.5) either as a part of a $k\alpha_0$ product or through homogeneous terms in $\boldsymbol{\alpha}$. Therefore, we can assume without a loss of generality that $\alpha_0 = 1$ and use k as the wave vector length. Note also that the Reynolds number Re enters (4.5) only as a part of a ratio k^2/Re. Denoting this ratio by μ, we rewrite (4.5) as

$$\left.\begin{aligned}
\dot{A}_1 &= -\tfrac{1}{2}\omega A_3 + \alpha_1(-\omega\alpha_3 A_1 + \omega\alpha_1 A_3) + \alpha_3\alpha_1 B - Fr\,\mu A_1,\\
\dot{A}_3 &= \tfrac{1}{2}\omega A_1 + \alpha_3(-\omega\alpha_3 A_1 + \omega\alpha_1 A_3) + \left(\alpha_3^2 - 1\right)B - Fr\,\mu A_3,\\
\dot{B} &= -b_1 A_1 - b_3 A_3 - Fr\,\mu Pr^{-1}B,
\end{aligned}\right\} \tag{4.6}$$

with

$$\boldsymbol{\alpha} = \begin{pmatrix} \sin(\phi)\sin(\theta(t) + \theta_0) \\ \cos(\phi) \\ -\sin(\phi)\cos(\theta(t) + \theta_0) \end{pmatrix}. \tag{4.7}$$

The parameters in the system above are $\theta_0, \phi, \mu, \mathscr{R}i, Pr$, where the Froude number Fr is related to the Richardson number via $\mathscr{R}i = 1/Fr^2$, according to (2.8) and (2.23). The first two parameters, θ_0 and ϕ, define the position of the perturbation wave vector $\boldsymbol{\alpha}$ at the initial time $t = 0$; the parameter $\mu = k^2/Re$ represents combined effects of viscosity and the wavenumber k, while Pr is responsible for the effects of heat conduction and $\mathscr{R}i$ is the Richardson number defined above in § 2. We investigate the influence of the parameters $\mathscr{R}i$, Pr, $\mu = k^2/Re$ and θ_0 on the stability properties of the nonlinear system (4.6). The second angular parameter ϕ is deliberately omitted for simplicity in exposition, since (as we will show later) it does not play a significant role in the stability analysis. As in §4.1, the strongest instabilities are located in the $\phi = \pi/2$ plane of the parameter space and are purely two-dimensional.

As in our earlier experiments for the inviscid, non-heat-conducting fluid, we tracked the trace of the fundamental matrix associated with (4.6) to determine whether or not the perturbations were stable. The large-scale vorticity ω was determined from the pendulum equations (2.17) and entered the equations as an external input.

We varied the Prandtl number from $Pr = 1$ to $Pr = 200$. These numbers roughly cover the range of physically relevant values. For each value of Pr we computed the trace of the fundamental matrix for (4.6) at Richardson numbers $\mathscr{R}i$ varying from 0.25 to 10. For each individual value of $\mathscr{R}i$ we present a contour diagram of trace in the (θ_0, μ)-plane. Then, we put together all such contour diagrams for Richardson numbers in the range specified above to create stability diagrams in the three variables

https://doi.org/10.1017/S0022112098003085 Published online by Cambridge University Press

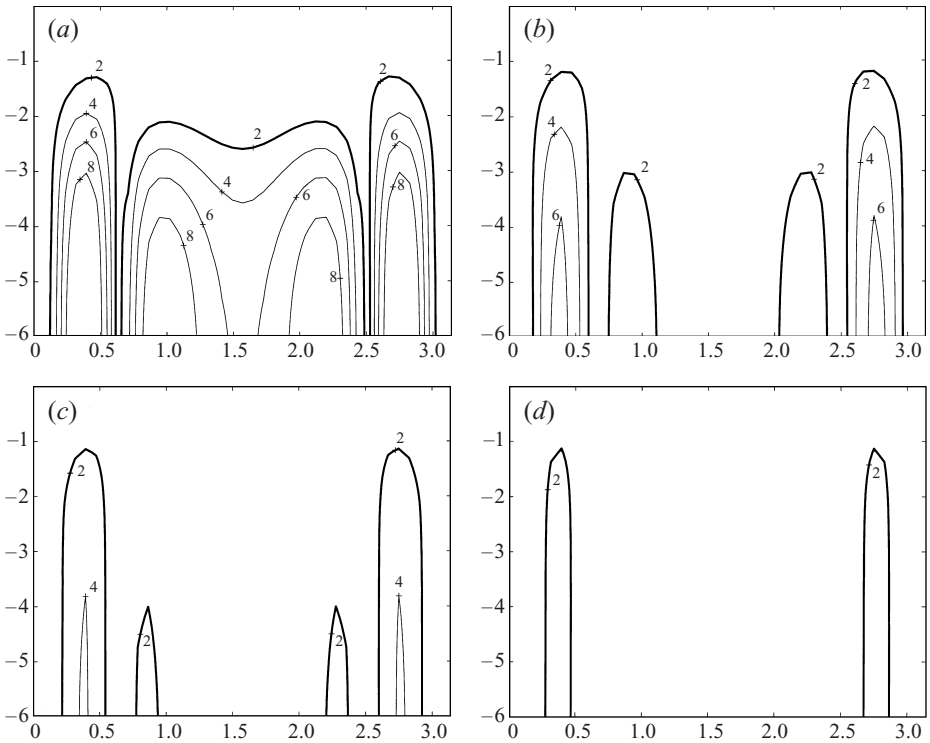


FIGURE 9. Effects of viscosity and heat conduction on instabilities at various Richardson numbers and Prandtl number, $Pr = 200$. The contours of fundamental matrix trace, $\mathrm{tr}\,\mathscr{R} = 2$ (bold curves), separate regions of stability and instability. The x-axis represents the θ_0-parameter while the y-axis is the parameter $\log(\mu)$, with $\mu = k^2/Re$ representing effective viscosity. The Richardson numbers depicted in (a), (b), (c), and (d) respectively are $\mathscr{R}i = 0.25, 0.5, 1$ and 3.

θ_0, μ and $\mathscr{R}i$. Surfaces shown on these three-dimensional diagrams separate stable and unstable regions. For $Pr = 200$, figure 9 shows contours of fundamental matrix trace in the (θ_0, μ)-plane for the specified values of Richardson number $\mathscr{R}i$. Figure 10 shows stability and instability regions in full $(\theta_0, \mu, \mathscr{R}i)$-space for $Pr = 200$.

In the numerical simulations we observed that flows with various values of Prandtl number, $Pr < 200$, exhibit qualitatively similar behaviour to the case $Pr = 200$; we omit the corresponding illustrations for brevity purposes.

We summarize our main conclusions as follows:

(a) Instabilities of two-dimensional plane wave perturbations to basic single vortex motions are present at all values of Richardson number, including those much larger than $\frac{1}{4}$;

(b) plane waves with large wavenumbers experience stronger dissipation by viscosity and heat conduction; however, instabilities are always present at sufficiently small values of the parameter $\mu = k^2/Re$;

(c) the Prandtl number Pr plays no significant role in the qualitative stability pictures for the range $1 \leqslant Pr \leqslant 200$.

Next, we illustrate that two-dimensional instabilities lying in the (x_1, x_3)-plane play the dominant role, exactly as in the inviscid, non-heat-conducting case. We present a few computations of the fundamental matrix trace when the parameters ϕ and θ_0 defining the wave vector $\boldsymbol{\alpha}$ (see (4.2)) both take the whole range of values between

https://doi.org/10.1017/S0022112098003085 Published online by Cambridge University Press

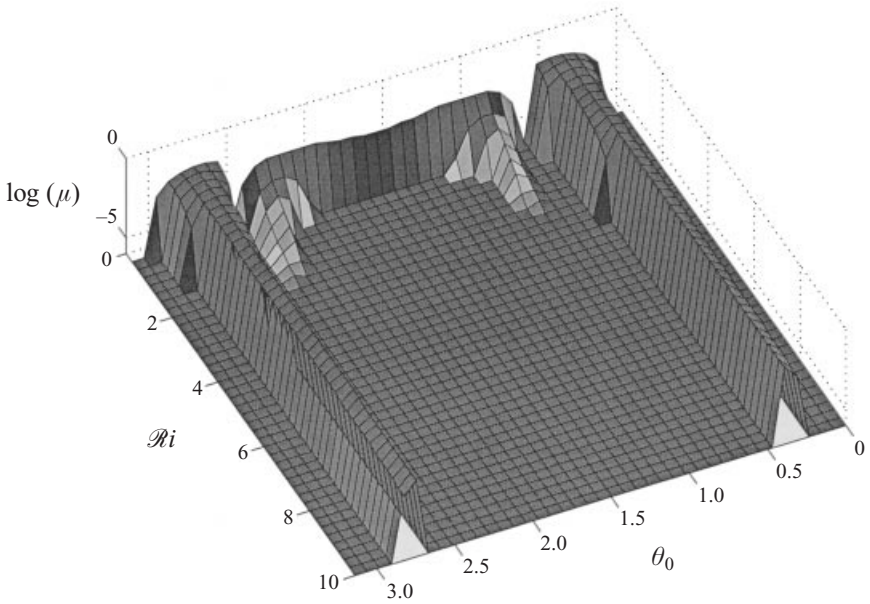


FIGURE 10. Effects of viscosity and heat conduction on instabilities at various Richardson numbers and Prandtl number, $Pr = 200$. The surface shown in this figure separates stability (above the surface) and instability (under the surface) regions.

0 and π, at several different values of the other parameters (μ, Re, Pr). The contour diagrams are shown in figure 11. These plots show that highest growth rates occur along the line $\phi = \pi/2, \alpha_2 = 0$, i.e. for the two-dimensional perturbations.

As in § 4.1, we comment on the physical nature of the instabilities discussed above. Single vortex flows are most unstable to two-dimensional plane wave perturbations in the (x_1, x_3)-plane. The strongest instabilities we have observed are growing oscillations with twice the period of the basic vortex motion. Perturbations with large enough wavenumbers k do not yield instabilities, since they get suppressed the most by the dissipative mechanisms.

5. Stability of vortex motions in a shear

In this section, we continue to study the stability of elementary flows introduced in § 2.1 and described by (2.6). In § 4 we restricted ourselves to the simple vortical flows with no vertical shear. Here, we investigate stability in the more general case, when both a vortex and a shear are present in the elementary flow, with and without the effects of viscosity and heat conduction.

5.1. *Stability of simple shears*

Here we check the stability of the simple shears (2.31) when $\mathscr{R}i > \frac{1}{4}$, with the definition of Richardson number $\mathscr{R}i$ introduced in and below (2.13) of § 2.2. The evolution equations (3.4) for the nonlinear perturbations of shears including viscosity

https://doi.org/10.1017/S0022112098003085 Published online by Cambridge University Press

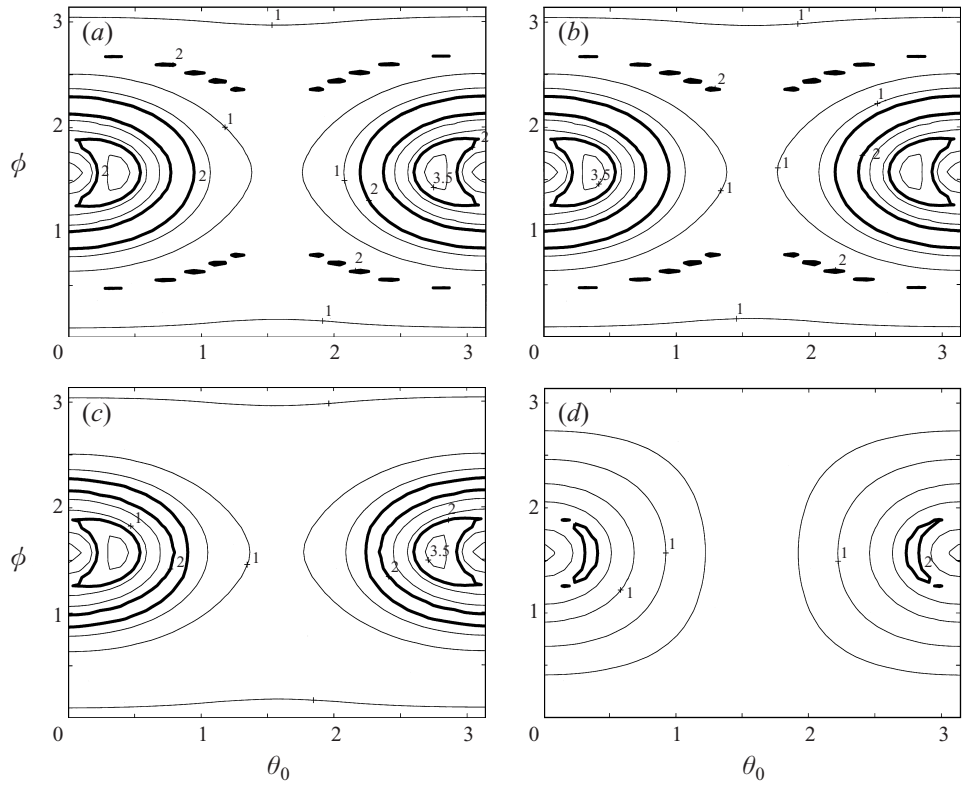


FIGURE 11. Regions of stability and instability for three-dimensional perturbations for different initial orientations of perturbation wave vector. The bold contours, tr $\mathscr{R} = 2$, separate stable and unstable regions. The parameters are (*a*) $\mathscr{R}i = 1,\ Pr = 1,\ \mu = 0.0001$, (*b*) $\mathscr{R}i = 1,\ Pr = 100,\ \mu = 0.0001$, (*c*) $\mathscr{R}i = 1,\ Pr = 10,\ \mu = 0.01$, and (*d*) $\mathscr{R}i = 10,\ Pr = 100,\ \mu = 0.1$.

and heat conduction effects take the following form:

$$\left.\begin{aligned}
&\dot{\alpha}_1 = 0, \quad \dot{\alpha}_2 = 0, \quad \dot{\alpha}_3 = -\sigma\alpha_1,\\
&\dot{A}_1 = -\sigma A_3 + 2\frac{\alpha_1^2}{|\boldsymbol{\alpha}|^2}\sigma A_3 + \frac{\alpha_1\alpha_3}{|\boldsymbol{\alpha}|^2}B - Fr\,Re^{-1}k^2|\boldsymbol{\alpha}|^2 A_1,\\
&\dot{A}_2 = 2\frac{\alpha_1\alpha_2}{|\boldsymbol{\alpha}|^2}\sigma A_3 + \frac{\alpha_2\alpha_3}{|\boldsymbol{\alpha}|^2}B - Fr\,Re^{-1}k^2|\boldsymbol{\alpha}|^2 A_2,\\
&\dot{A}_3 = 2\frac{\alpha_1\alpha_3}{|\boldsymbol{\alpha}|^2}\sigma A_3 + \left(\frac{\alpha_3^2}{|\boldsymbol{\alpha}|^2} - 1\right)B - Fr\,Re^{-1}k^2|\boldsymbol{\alpha}|^2 A_3,\\
&\dot{B} = A_3 - Fr\,Pr^{-1}Re^{-1}k^2|\boldsymbol{\alpha}|^2 B.
\end{aligned}\right\} \tag{5.1}$$

We note that the Froude number for the elementary shear flows (2.31) is related to the Richardson number through $\mathscr{R}i = 2/(3\sigma^2) = 2/(3Fr^2)$. The equations for the wave vector $\boldsymbol{\alpha}$ can be easily solved in this case,

$$\alpha_1(t) = \alpha_1^*, \quad \alpha_2(t) = \alpha_2^*, \quad \alpha_3(t) = \alpha_3^* - \sigma\alpha_1^* t. \tag{5.2}$$

https://doi.org/10.1017/S0022112098003085 Published online by Cambridge University Press

Since the equations for $A_3(t)$ and $B(t)$ decouple from the first two amplitude equations in (5.1), we will focus our consideration on the stability of A_3 and B. The two other perturbation amplitudes, $A_1(t)$ and $A_2(t)$, turn out to be slave modes and cause no additional instabilities. When $\alpha_1^* = 0$ and the effects of diffusion are ignored, the amplitude equations take an especially simple form,

$$\left.\begin{aligned} \dot{A}_3 &= \left(\frac{(\alpha_3^*)^2}{(\alpha_2^*)^2 + (\alpha_3^*)^2} - 1\right) B, \\ \dot{B} &= A_3. \end{aligned}\right\} \tag{5.3}$$

Clearly, (5.3) produce stable oscillations with the frequency $(1-(\alpha_3^*)^2/((\alpha_2^*)^2+(\alpha_3^*)^2))^{1/2}$ provided $\alpha_2^* \neq 0$. It is easy to check that the two other amplitudes, A_1 and A_2, in this case also exhibit oscillatory behaviour. A very special set of solutions arises when both α_1^* and α_2^* are set equal to zero. Here, vertical shears of horizontal velocity v_1 are perturbed in the vertical direction and typically produce a linear growth in time (the vertical component of the perturbation velocity A_3 needs to be non-zero). This type of instability for stratified shear flows has been discussed earlier by Criminale & Cordova (1986). We emphasize that marginal linear instability of this type differs greatly from the exponential instability of simple vortices we observed in §§4.1 and 4.2 and is typically destroyed by arbitrarily small dissipation. The existence of this marginally stable growing mode with α_1^* and α_2^* vanishing does not contradict the Miles–Howard theorem for $\mathscr{R}i > \frac{1}{4}$; the Miles–Howard theorem involves flow fields which are bounded by parallel walls in the vertical direction where the normal velocity of the fluid flow must vanish and these vertically propagating modes clearly violate the boundary conditions.

According to the Miles–Howard theorem, we anticipate that all shears with σ (or, equivalently, Fr) smaller than a certain cut-off value must be stable. Since the definition of the Richardson number differs from the traditional definition via the vertical gradient of horizontal velocity used by Miles and Howard, equal in our case to $1/\sigma^2$, it is very natural to pick $\sigma = 2$ as the critical value defining $\mathscr{R}i = \frac{1}{4}$. We have numerically investigated the stability of shears with several values of $\sigma < 2$ with an emphasis on non-normal transient growth at moderate times. Our calculations confirm that shears are always marginally stable. In the inviscid, non-heat-conducting case there is a special mode, with amplitudes growing linearly in time, corresponding to perturbations with $\alpha_2 = 0$. In a typical perturbation with α_2^* different from zero, we observed a considerable transient growth; solutions then eventually levelled off. The non-trivial α_2-component in a wave vector tends to stabilize the flow. We omit detailed figures demonstrating these effects. The special mode is isolated, since even a small amount of noise in the α_2-component of the wave vector destroys it by generating rapid large-amplitude oscillations. It is clear that the special mode can also be destroyed by dissipation as noted earlier (Criminale & Cordova 1986).

Except for the special mode, the simple shears with $\mathscr{R}i > \frac{1}{4}$ are stable to plane wave perturbations. In the next section we will study the stability of general elementary flows described in § 2.4, involving both shear and vortex motion. Some of the perturbations exhibit non-normal behaviour, with substantial transient growth over relatively few buoyancy times. A useful gauge of the stability properties of elementary flows is given by the ratio

$$r_{max} = \max_{t>0} \frac{|\boldsymbol{C}(t)|}{|\boldsymbol{C}(0)|}, \tag{5.4}$$

https://doi.org/10.1017/S0022112098003085 Published online by Cambridge University Press

where $\boldsymbol{C}(t)$ is the vector of perturbation amplitudes. To quantify the non-normal transient growth at short times, we use the typical value of r_{max} for shears in the interval $0 \leqslant t \leqslant 50$; it roughly equals 50. We used this value as a threshold to separate solutions with stable ($r_{max} < 50$) and significantly non-normal ($r_{max} > 50$) behaviour in a fashion consistent with the stability of shear flows. Clearly, the shear flows themselves are always stable with this definition.

5.2. *Stability of perturbations to general elementary flows*

The most general case of the elementary flows (2.6) involves both a vortical and a shear component. There, (3.4) describe the time evolution of the perturbation wave vector $\boldsymbol{\alpha}$, velocity and density amplitudes $\boldsymbol{A}$ and B, and take the following form:

$$\left.\begin{aligned}
&\dot{\alpha}_1 = \frac{\omega-\sigma}{2}\alpha_3, \quad \dot{\alpha}_3 = -\frac{\omega+\sigma}{2}\alpha_1,\\
&\dot{A}_1 = -\frac{\omega+\sigma}{2}A_3 + \frac{\alpha_1}{|\boldsymbol{\alpha}|^2}\left(A_1\alpha_3(\sigma-\omega) + A_3\alpha_1(\sigma+\omega)\right)\\
&\qquad + \frac{\alpha_1\alpha_3}{|\boldsymbol{\alpha}|^2}B - Fr\,Re^{-1}k^2|\boldsymbol{\alpha}|^2A_1,\\
&\dot{A}_3 = \frac{\omega-\sigma}{2}A_1 + \frac{\alpha_3}{|\boldsymbol{\alpha}|^2}\left(A_1\alpha_3(\sigma-\omega) + A_3\alpha_1(\sigma+\omega)\right)\\
&\qquad + \left(\frac{\alpha_3^2}{|\boldsymbol{\alpha}|^2} - 1\right)B - Fr\,Re^{-1}k^2|\boldsymbol{\alpha}|^2A_3,\\
&\dot{B} = -A_1b_1 - A_3b_3 - Fr\,Pr^{-1}Re^{-1}k^2|\boldsymbol{\alpha}|^2B.
\end{aligned}\right\} \tag{5.5}$$

The Richardson number for general elementary flows (2.6) is defined in §2.2 and can be recovered for each value of the Froude number and the strain parameter σ. The contour diagram of the Richardson number in the (Fr, σ)-plane is shown in figure 4.

The equations above are purely nonlinear; therefore, the simplifications which lead to the use of Floquet theory for the simple vortex case considered earlier in §4 are no longer applicable. Instead, we perform direct numerical simulations of (5.5). Since α_2 and A_2 decouple from the rest of the variables, we omit them for simplicity. In our simulations, we selected a few 'typical' values of the Richardson number, ranging over $\mathscr{R}i = 0.25, 1, 3, 5, 10$. For each of these values we picked several pairs (Fr, σ) generating elementary solutions with the selected Richardson number (such pairs lie on the level lines of Richardson number shown in figure 4.

First we consider the situation without viscosity and heat conduction. It clearly follows from the last three equations in (5.5) that the length of a perturbation wave vector $|\boldsymbol{\alpha}|$ is irrelevant for the stability studies, since $\boldsymbol{\alpha}$ enters the equations only through homogeneous terms in $\boldsymbol{\alpha}$. Therefore, it is sufficient to consider initial conditions for $\boldsymbol{\alpha}$ in the form of a unit vector, with the two angular parameters ϕ and θ_0 defining its initial direction. Our simulations demonstrated that the parameter ϕ, describing initial deflection of the wave vector from the (x_1, x_3)-plane, does not lead to the most unstable modes and therefore can be omitted for simplicity. For the perturbation amplitudes, we restricted initial conditions to the following 'typical' sets:

$$(A_1, A_3, B) = \begin{cases} (1,0,0)\\ (0,1,0)\\ (0,0,1). \end{cases}$$

https://doi.org/10.1017/S0022112098003085 Published online by Cambridge University Press

To investigate the stability of an elementary solution corresponding to a pair (Fr, σ) we used forty homogeneously spaced directions of a wave vector $\boldsymbol{\alpha}$ in the (x_1, x_3)-plane, along with the initial conditions for the perturbation amplitudes A_1, A_3, B as above.

Here is the summary of our study in the inviscid, non-heat-conducting case:

(i) Of all elementary flows we have considered, only the vortex flows (2.14) are genuinely (exponentially) unstable to the plane wave perturbations in the absence of viscosity and heat conduction.

(ii) Two-dimensional perturbations located in the (x_1, x_3)-plane ($\alpha_2 = 0$) always produce the most significant growth.

(iii) Perturbations to all elementary solutions with $\sigma \neq 0$ have a special marginally stable mode. It corresponds to perturbations with initial conditions $\boldsymbol{\alpha}(0) = (0, 0, \alpha_3(0))$. For flows with small Richardson number (with a typical $\mathscr{R}i$ smaller than 0.1) this mode is exponentially unstable, but as the Richardson number increases, this mode converges to a linear growth. This special mode is easily destroyed by even a tiny amount of the α_2-component. These deflections of the wave vector from the (x_1, x_3)-plane generate large amplitude fluctuations at larger times saturating to a constant or to stable oscillations.

(iv) There exists a set of elementary flows, whose perturbations present substantial (exponential) transient growth at short times and then level off. Corresponding to the pure vortical flows of § 4, these flows are located in a strip in the (Fr, σ)-plane around the line $\sigma = 0$. The width of the strip with such non-normal behaviour changes with the Richardson number, increasing for the small values of $\mathscr{R}i$. The approximate width of this region measured with respect to the threshold, r_{max} from (5.4) satisfying $r_{max} > 50$, introduced above is equal to

$$\left.\begin{aligned} |\sigma| &\leqslant 0.5 \text{ for } \mathscr{R}i = 1, \\ |\sigma| &\leqslant 0.1 \text{ for } \mathscr{R}i = 5, \\ |\sigma| &\leqslant 0.05 \text{ for } \mathscr{R}i = 10. \end{aligned}\right\} \tag{5.6}$$

Effect of viscosity and heat conduction

In the presence of viscosity and heat conduction for solutions of the system (5.5), the length of the wave vector $\boldsymbol{\alpha}$ changes in time. In fact, the numerical experiments demonstrate that $|\boldsymbol{\alpha}|$ grows roughly linearly in time. According to (5.5), this growth enhances the influence of the dissipative forces. Direct numerical integration of the system (5.5) confirms that viscosity is much more effective at large Richardson numbers in suppressing non-normal growth in the region with substantial non-normal behaviour described in (5.6).

6. Concluding discussion

We briefly summarize the main results contained in this paper. The elementary time-periodic stratified flows with vorticity and no strain flow given in (1.2) and (1.3) are unstable at all Richardson numbers. As documented in § 4, parametric two-dimensional instability is the dominant mode of growth and this behaviour persists for all Reynolds numbers and a wide range of Prandtl numbers. In order to understand the robustness of the phenomena present in this instability and its potential physical significance, it is of interest to assess the occurrence of similar instabilities in a

https://doi.org/10.1017/S0022112098003085 Published online by Cambridge University Press

wider class of elementary stratified flow fields. Thus, in §5, we extended the stability considerations to the most general case of elementary stratified flows described in (2.6). The elementary flows with non-zero strain are always (marginally) stable and never exhibit exponential amplification of perturbations at arbitrarily long times for the wide range of Froude numbers and strain rates tested. As for the case of shear flows (Criminale & Cordova 1986) the elementary flows of general form have a special marginal mode, with perturbation amplitudes growing linearly in time (in the absence of dissipative effects). In addition to this effect, suitable perturbations of elementary solutions located in a band in the (Fr, σ)-plane near the line $\sigma = 0$ experience substantial exponential growth at short times and then level off. This regime of elementary flows was described in § 5 through quantitative comparison with transient behaviour in shear flows. Such elementary flows with significant non-normal transient behaviour become important in the framework of the full Boussinesq equations where the large perturbation amplitudes in the short-time regime can trigger nonlinear mechanisms of instability which cannot be explained by linear theory.

In the elementary flows introduced in § 2 with either nonlinear instability or non-normal transient growth at large Richardson numbers, it is obviously very interesting to determine the nonlinear saturation of such instabilities through careful numerical simulation. In a preliminary numerical study Majda & Shefter (1998) examined the nonlinear saturation of instability for the elementary flows (1.2) and (1.3) for $\mathscr{R}i = 5$. Substantial local density overturning with nonlinear Kelvin–Helmholtz instability developed spontaneously from random initial data through the linearized instability mechanism described here.

The consequences of the nonlinear saturation of the linear instabilities discussed here regarding overturning and mixing are the important physical facts needed in a quantitative assessment of the effectiveness of the Lilly–Smagorinsky eddy diffusivity in stably stratified flow as well as potential improvements for large-eddy simulations. The authors are currently investigating these issues through detailed numerical simulation which will be reported elsewhere.

Appendix. Derivation of exact solution identities

In this Appendix we show the existence of a family of exact solutions to the Boussinesq equations by generalizing the procedure of Craik & Criminale (1986). We then systematically derive the (ordinary differential) equations that simplified terms in these solutions must satisfy in order for the Boussinesq equations to hold. We start with non-rotating Boussinesq equations with viscosity and heat conduction:

$$\left.\begin{aligned} \frac{\mathrm{D}\boldsymbol{v}}{\mathrm{D}t} &= -\nabla p - \frac{g}{\rho_b}\rho \boldsymbol{e}_3 + \nu \Delta \boldsymbol{v}, \\ \operatorname{div} \boldsymbol{v} &= 0, \\ \frac{\mathrm{D}\tilde{\rho}}{\mathrm{D}t} &= \kappa \Delta \tilde{\rho} \end{aligned}\right\} \tag{A 1}$$

(where $\rho = \rho_b + \tilde{\rho}$) and assume that there exist exact solutions in the form of superposition of linear-in-space solutions and nonlinear plane waves:

$$\left.\begin{aligned} \boldsymbol{v}(\boldsymbol{x}, t) &= \mathscr{D}(t)\boldsymbol{x} + \tfrac{1}{2}\boldsymbol{\omega}(t) \times \boldsymbol{x} + \boldsymbol{A}(t)F(\boldsymbol{\alpha}(t) \cdot \boldsymbol{x}), \\ \tilde{\rho}(\boldsymbol{x}, t) &= \rho_b + \boldsymbol{b}(t) \cdot \boldsymbol{x} + B(t)F'(\boldsymbol{\alpha}(t) \cdot \boldsymbol{x}), \\ p(\boldsymbol{x}, t) &= \tfrac{1}{2}\hat{\boldsymbol{P}}(t)\boldsymbol{x} \cdot \boldsymbol{x} + P(t)G(\boldsymbol{\alpha}(t) \cdot \boldsymbol{x}). \end{aligned}\right\} \tag{A 2}$$

https://doi.org/10.1017/S0022112098003085 Published online by Cambridge University Press

Here, the relationships among the waveform functions $F(s), F'(s)$ and $G(s)$ are to be determined; $\mathscr{D}(t)$ is an arbitrary 3×3 symmetric matrix, so that $\boldsymbol{\omega} = \operatorname{curl} \boldsymbol{v}$. We introduce the antisymmetric matrix Ω by the relation $\boldsymbol{\omega}(t) \times \boldsymbol{x} = \Omega(t)\boldsymbol{x}$. Let the matrix $\boldsymbol{V} = \mathscr{D} + \Omega$ so that

$$\boldsymbol{v}(\boldsymbol{x}, t) = \boldsymbol{V}(t)\boldsymbol{x} + \boldsymbol{A}(t)F(\boldsymbol{\alpha} \cdot \boldsymbol{x}). \tag{A 3}$$

The first constraint is incompressibility, the second equation in (A 1), which under the ansatz, (A 2), becomes $\operatorname{div} \boldsymbol{v} = \operatorname{tr} \mathscr{D} + \boldsymbol{A} \cdot \boldsymbol{\alpha} F'$. As F is arbitrary, we must require that $\mathscr{D}$ be trace free,

Condition 1: $$\operatorname{tr} \mathscr{D}(t) = 0$$

and enforce the remaining condition

$$\boldsymbol{A}(t) \cdot \boldsymbol{\alpha}(t) = 0 \tag{A 4}$$

for all times. This will not yet be required, as we need to see how $\boldsymbol{\alpha}$ evolves in a divergence-free field in order to determine a suitable condition. So we will assume this fact for now and later show it to be true. Looking now at the density equation, the third in (A 1), we find

$$\begin{aligned} 0 &= -\kappa \Delta \tilde{\rho} + \frac{\mathrm{D}\tilde{\rho}}{\mathrm{D}t} \\ &= \frac{\mathrm{d}\boldsymbol{b}}{\mathrm{d}t} \cdot \boldsymbol{x} + \frac{\mathrm{d}B}{\mathrm{d}t}\tilde{F} + B\frac{\mathrm{d}\boldsymbol{\alpha}}{\mathrm{d}t} \cdot \boldsymbol{x}\tilde{F}' + \boldsymbol{v} \cdot \boldsymbol{b} + B\boldsymbol{v} \cdot \boldsymbol{\alpha}\tilde{F}' - \kappa B|\boldsymbol{\alpha}|^2\tilde{F}''. \end{aligned}$$

If we insert our ansatz, (A 2), for $\boldsymbol{v}$ into this equation, we find

$$\begin{aligned} 0 = &\left(\frac{\mathrm{d}\boldsymbol{b}}{\mathrm{d}t} + \boldsymbol{V}^T\boldsymbol{b}\right) \cdot \boldsymbol{x} + \left(\frac{\mathrm{d}B}{\mathrm{d}t} + \boldsymbol{A} \cdot \boldsymbol{b}\right)\tilde{F} + B\left(\frac{\mathrm{d}\boldsymbol{\alpha}}{\mathrm{d}t} + \boldsymbol{V}^T\boldsymbol{\alpha}\right) \cdot \boldsymbol{x}\tilde{F}' \\ &- \left(\kappa|\boldsymbol{\alpha}|^2 B\right)\tilde{F}'' + B(\boldsymbol{A} \cdot \boldsymbol{\alpha})\tilde{F}\tilde{F}'. \end{aligned} \tag{A 5}$$

By the incompressibility condition in (A 4) the last term is identically zero. In order to balance the term proportional to $\tilde{F}''$, we will need to assume it is identically zero or else proportional to one of the other groups of terms in the equation. Choosing $\tilde{F}'' = 0$ would amount to choosing $\tilde{F}(y) = cy$, which yields perturbations unbounded in space, a physically unreasonable assumption. Similarly, choosing $\tilde{F}'' = \pm k\tilde{F}'$ or $\tilde{F}'' = k^2\tilde{F}$ would lead to solutions $\tilde{F}(y) = \mathrm{e}^{\pm ky}$ which would be unbounded and thus unacceptable. We are therefore led to the additional assumption:

Condition 2: $$\tilde{F}'' = -k^2\tilde{F}.$$

Hence, $\tilde{F}$ must be sinusoidal with wavenumber k,

$$\tilde{F}(y) = \cos(ky - \theta_0).$$

This equation thus reduces to

$$0 = \left(\frac{\mathrm{d}\boldsymbol{b}}{\mathrm{d}t} + \boldsymbol{V}^T\boldsymbol{b}\right) \cdot \boldsymbol{x} + \left(\frac{\mathrm{d}B}{\mathrm{d}t} + \boldsymbol{A} \cdot \boldsymbol{b} + k^2\kappa|\boldsymbol{\alpha}|^2 B\right)\tilde{F} + B\left(\frac{\mathrm{d}\boldsymbol{\alpha}}{\mathrm{d}t} + \boldsymbol{V}^T\boldsymbol{\alpha}\right) \cdot \boldsymbol{x}\tilde{F}'. \tag{A 6}$$

The three groups of terms are linearly independent and must be separately set to zero, leading to the three equations for $\boldsymbol{b}$, B, and $\boldsymbol{\alpha}$:

Condition 3: $$\frac{\mathrm{d}\boldsymbol{b}}{\mathrm{d}t} = \mathscr{D}(t)\boldsymbol{b}(t) + \tfrac{1}{2}\boldsymbol{\omega}(t) \times \boldsymbol{b}(t),$$

https://doi.org/10.1017/S0022112098003085 Published online by Cambridge University Press

Condition 4: $$\frac{\mathrm{d}B}{\mathrm{d}t} = -\boldsymbol{b}(t)\cdot\boldsymbol{A}(t) - \kappa k^2|\boldsymbol{\alpha}|^2 B,$$

Condition 5: $$\frac{\mathrm{d}\boldsymbol{\alpha}}{\mathrm{d}t} = -\boldsymbol{V}^T(t)\boldsymbol{\alpha}(t).$$

We now compute the velocity terms of the momentum equation (the first equation in (A 1)):

$$\begin{aligned}\frac{\partial \boldsymbol{v}}{\partial t} &= \frac{\mathrm{d}\boldsymbol{V}}{\mathrm{d}t}\boldsymbol{x} + \frac{\mathrm{d}\boldsymbol{A}}{\mathrm{d}t}F + \boldsymbol{A}\frac{\mathrm{d}\boldsymbol{\alpha}}{\mathrm{d}t}\cdot\boldsymbol{x}F',\\ \boldsymbol{v}\cdot\nabla\boldsymbol{v} &= \boldsymbol{v}\cdot\boldsymbol{V} + \boldsymbol{A}(\boldsymbol{V}\boldsymbol{x}\cdot\boldsymbol{\alpha})F'\\ &= \boldsymbol{V}^2\boldsymbol{x} + \boldsymbol{A}\cdot\boldsymbol{V}F + \boldsymbol{A}(\boldsymbol{V}\boldsymbol{x}\cdot\boldsymbol{\alpha})F' + \boldsymbol{A}(\boldsymbol{A}\cdot\boldsymbol{\alpha})FF',\\ \nu\Delta\boldsymbol{v} &= \nu|\boldsymbol{\alpha}|^2F''\boldsymbol{A}.\end{aligned}$$

Again the last term in the convective part is identically zero because of the incompressibility condition (A 4). The pressure and density terms in the equations are

$$\nabla p = \hat{\boldsymbol{P}}\boldsymbol{x} + P\boldsymbol{\alpha}G', \tag{A 7}$$

$$\frac{g\rho}{\rho_b}\boldsymbol{e}_3 = \frac{g}{\rho_b}(\boldsymbol{b}\otimes\boldsymbol{e}_3)\boldsymbol{x} + \frac{g}{\rho_b}B\boldsymbol{e}_3\tilde{F}. \tag{A 8}$$

Combining these terms, we reduce the momentum equation to

$$\left(\frac{\mathrm{d}\boldsymbol{V}}{\mathrm{d}t} + \boldsymbol{V}^2 + \hat{\boldsymbol{P}} + \boldsymbol{b}\otimes\boldsymbol{e}_3\right)\boldsymbol{x} + \left(\frac{\mathrm{d}\boldsymbol{A}}{\mathrm{d}t} + \boldsymbol{A}\cdot\boldsymbol{V}\right)F + P\boldsymbol{\alpha}G' + \frac{gB}{\rho_b}\boldsymbol{e}_3\tilde{F} + \boldsymbol{A}\left(\frac{\mathrm{d}\boldsymbol{\alpha}}{\mathrm{d}t} + \boldsymbol{V}^T\boldsymbol{\alpha}\right)\cdot\boldsymbol{x}F' = \nu|\boldsymbol{\alpha}|^2F''\boldsymbol{A}. \tag{A 9}$$

Note that the coefficient of F' in the above is identically zero by Condition 5. This equation must hold for arbitrary F and G, so that the coefficient of $\boldsymbol{x}$ must be forced to vanish. Equation (A 9) can be separated into a symmetric and anti-symmetric parts, which form the next two conditions.

Condition 6: $$\frac{\mathrm{d}\boldsymbol{\omega}}{\mathrm{d}t} = \mathscr{D}(t)\boldsymbol{\omega}(t) + \frac{g}{\rho_b}\begin{pmatrix}-b_2\\ b_1\\ 0\end{pmatrix},$$

Condition 7: $$-\hat{\boldsymbol{P}} = \frac{\mathrm{d}\mathscr{D}}{\mathrm{d}t} + \mathscr{D}(t)^2 + \Omega(t)^2 + \frac{g}{2\rho_b}(\boldsymbol{e}_3\otimes\boldsymbol{b} + \boldsymbol{b}\otimes\boldsymbol{e}_3).$$

This serves to define $\hat{\boldsymbol{P}}(t)$ in terms of other variables which participate directly in the dynamics.

The remaining part of the momentum equation (A 9) is thus

$$\left(\frac{\mathrm{d}\boldsymbol{A}}{\mathrm{d}t} + \boldsymbol{A}\cdot\boldsymbol{V}\right)F + P\boldsymbol{\alpha}G' + \frac{gB}{\rho_b}\boldsymbol{e}_3\tilde{F} = \nu|\boldsymbol{\alpha}|^2F''\boldsymbol{A}.$$

Then the necessary relationship among the waveforms must be

Condition 8: $$F(y) = \tilde{F}(y) = G'(y) = \frac{-F''(y)}{k^2} = \cos(ky - \theta_0).$$

This relationship yields that

$$\frac{\mathrm{d}\boldsymbol{A}}{\mathrm{d}t} + \boldsymbol{A}\cdot\boldsymbol{V} + P\boldsymbol{\alpha} + \frac{gB}{\rho_b} = -\nu k^2|\boldsymbol{\alpha}|^2\boldsymbol{A}. \tag{A 10}$$

https://doi.org/10.1017/S0022112098003085 Published online by Cambridge University Press

The last expression still contains the pressure P which we may eliminate as a dynamical variable as follows. Returning to the divergence-free condition, we first enforce that our initial condition is divergence free,

Condition 9: $$\boldsymbol{\alpha}\cdot\boldsymbol{A}|_{t=0}=0,$$

and then for it to remain zero its derivative must vanish

$$\frac{\mathrm{d}}{\mathrm{d}t}(\boldsymbol{A}\cdot\boldsymbol{\alpha})=0.$$

Now we may use Condition 5 and (A 10) to obtain

$$-\left(\frac{\mathrm{d}\boldsymbol{A}}{\mathrm{d}t}\cdot\boldsymbol{\alpha}+\boldsymbol{A}\cdot\frac{\mathrm{d}\boldsymbol{\alpha}}{\mathrm{d}t}\right)=(\boldsymbol{V}\boldsymbol{A})\cdot\boldsymbol{\alpha}+P|\boldsymbol{\alpha}|^2+\frac{gB}{\rho_b}\alpha_3+\boldsymbol{A}\cdot(\boldsymbol{V}^T\boldsymbol{\alpha})+\nu k^2|\boldsymbol{\alpha}|^2\boldsymbol{A}\cdot\boldsymbol{\alpha}.$$

Note that for consistency, the final term must be set to zero, so that the pressure is unchanged from before:

Condition 10: $$-P(t)=\frac{2(\boldsymbol{V}^T\boldsymbol{\alpha}\cdot\boldsymbol{A})}{|\boldsymbol{\alpha}|^2}+\frac{g}{\rho_b}\frac{B\alpha_3}{|\boldsymbol{\alpha}|^2}+\nu k^2\boldsymbol{A}\cdot\boldsymbol{\alpha}.$$

Inserting the expression for the pressure back in the equation for $\boldsymbol{A}$ yields our final condition:

Condition 11: $$\frac{\mathrm{d}\boldsymbol{A}}{\mathrm{d}t}=-\boldsymbol{V}\boldsymbol{A}+\boldsymbol{\alpha}\frac{2(\boldsymbol{V}^T\boldsymbol{\alpha}\cdot\boldsymbol{A})}{|\boldsymbol{\alpha}|^2}+\frac{g}{\rho_b}\left[\frac{\alpha_3}{|\boldsymbol{\alpha}|^2}\boldsymbol{\alpha}-\boldsymbol{e}_3\right]B-\nu k^2|\boldsymbol{\alpha}|^2\boldsymbol{A}.$$

In summary, we have proven the following:

THEOREM 1. *The viscous, heat-conducting Boussinesq equations in* (A 1) *have special solutions of the form*

$$\left.\begin{aligned}\boldsymbol{v}(\boldsymbol{x},t)&=\mathscr{D}(t)\boldsymbol{x}+\tfrac{1}{2}\boldsymbol{\omega}(t)\times\boldsymbol{x}+\boldsymbol{A}(t)F(\boldsymbol{\alpha}\cdot\boldsymbol{x}),\\ \tilde{\rho}(\boldsymbol{x},t)&=\rho_b+\boldsymbol{b}\cdot\boldsymbol{x}+B(t)F(\boldsymbol{\alpha}\cdot\boldsymbol{x}),\\ p(\boldsymbol{x},t)&=\tfrac{1}{2}\hat{\boldsymbol{P}}(t)\boldsymbol{x}\cdot\boldsymbol{x}+P(t)G(\boldsymbol{\alpha}\cdot\boldsymbol{x}),\end{aligned}\right\}\tag{A 11}$$

provided the following conditions hold:

$$\left.\begin{aligned}&\operatorname{tr}\mathscr{D}(t)=0,\quad \boldsymbol{\alpha}\cdot\boldsymbol{A}|_{t=0}=0,\quad F(y)=G'(y)=\cos(ky-\theta_0),\\ &\frac{\mathrm{d}\boldsymbol{b}}{\mathrm{d}t}=\mathscr{D}(t)\boldsymbol{b}(t)+\tfrac{1}{2}\boldsymbol{\omega}(t)\times\boldsymbol{b}(t),\quad \frac{\mathrm{d}B}{\mathrm{d}t}=-\boldsymbol{b}(t)\cdot\boldsymbol{A}(t)-\kappa k^2|\boldsymbol{\alpha}|^2B,\\ &\frac{\mathrm{d}\boldsymbol{\alpha}}{\mathrm{d}t}=-\boldsymbol{V}^T(t)\boldsymbol{\alpha}(t),\quad \frac{\mathrm{d}\boldsymbol{\omega}}{\mathrm{d}t}=\mathscr{D}(t)\boldsymbol{\omega}(t)+\frac{g}{\rho_b}\begin{pmatrix}-b_2\\ b_1\\ 0\end{pmatrix},\\ &\frac{\mathrm{d}\boldsymbol{A}}{\mathrm{d}t}=-\boldsymbol{V}\boldsymbol{A}+\boldsymbol{\alpha}\frac{2(\boldsymbol{V}^T\boldsymbol{\alpha}\cdot\boldsymbol{A})}{|\boldsymbol{\alpha}|^2}+\frac{g}{\rho_b}\left[\frac{\alpha_3}{|\boldsymbol{\alpha}|^2}\boldsymbol{\alpha}-\boldsymbol{e}_3\right]B-\nu k^2|\boldsymbol{\alpha}|^2\boldsymbol{A},\end{aligned}\right\}\tag{A 12}$$

https://doi.org/10.1017/S0022112098003085 Published online by Cambridge University Press

in which case the pressure can be recovered from

$$\left.\begin{aligned} -\hat{\boldsymbol{P}} &= \frac{\mathrm{d}\mathscr{D}}{\mathrm{d}t} + \mathscr{D}(t)^2 + \Omega(t)^2 + \frac{g}{2\rho_b}\left(\boldsymbol{e}_3 \otimes \boldsymbol{b} + \boldsymbol{b} \otimes \boldsymbol{e}_3\right), \\ -P(t) &= \frac{2(\boldsymbol{V}^T\boldsymbol{\alpha}\cdot\boldsymbol{A})}{|\boldsymbol{\alpha}|^2} + \frac{g}{\rho_b}\frac{B\alpha_3}{|\boldsymbol{\alpha}|^2} + \nu k^2 \boldsymbol{A}\cdot\boldsymbol{\alpha}, \\ \boldsymbol{V}(t) &= \mathscr{D}(t) + \Omega(t), \end{aligned}\right\} \tag{A 13}$$

with $\Omega\boldsymbol{h} = \frac{1}{2}\boldsymbol{\omega}\times\boldsymbol{h}$ *for any* $\boldsymbol{h}$.

Remark. The same analysis holds for the exact solutions of the inviscid, non-heat-conducting Boussinesq equations with only one modification. One does not have to require waveform function $F(y)$ to be sinusoidal (compare with Condition 2); in fact, any smooth function $F(y)$ will satisfy the Boussinesq equations.

Andrew Majda is partially supported by research grants, NSF DMS-9625795, ONR N00014-96-0043, ARO DAAH04-95-1-0345. Michael Shefter is supported as a post-doc through grants NSF DMS-9625795, ONR N00014-96-0043.

REFERENCES

Bayly, B. J. 1986 Three-dimensional instability of elliptical flow. *Phys. Rev. Lett.* **57**, 2160–2163.

Bayly, B. J., Holm, D. D. & Lifschitz, A. 1996 Three-dimensional stability of elliptical vortex columns in external strain flows. *Phil. Trans. R. Soc. Lond.* A **354**, 895–926.

Bretherton, C. S., MacVean, M. K., Bechtold, P., Chlond, A., Cotton, W. R., Cuxart, J., Cuijpers, H., Khairoutdinov, M., Kosovic, B., Lewellen, D., Moeng, C.-H., Siebesma, P., Stevens, B., Stevens, D. E., Sykes, I. & Wyant, M. C. 1998 An intercomparison of radiatively-driven entrainment and turbulence in a smoke cloud, as simulated by different numerical models. Submitted to *Q. J. R. Met. Soc.*

Craik, A. D. D. 1989 The stability of unbounded two- and three-dimensional flows subject to body forces: some exact solutions. *J. Fluid Mech.* **198**, 275–292.

Craik, A. D. D. & Allen, H. R. 1992 The stability of three-dimensional time-periodic flows with spatially uniform strain rates. *J. Fluid Mech.* **234**, 613–628.

Craik, A. D. D. & Criminale, W. O. 1986 Evolution of wavelike disturbances in shear flows: a class of exact solutions of the Navier-Stokes equations. *Proc. R. Soc. Lond.* A **406**, 13–26.

Criminale, W. O. & Cordova, J. Q. 1986 Effects of diffusion in the asymptotics of perturbations in stratified shear flow. *Phys. Fluids* **29**, 2054–2060.

Drazin, P. G. 1977 On the instability of an internal gravity wave. *Proc. R. Soc. Lond.* A **356**, 411–432.

Farrell, B. & Ioannou, P. 1993 Perturbation growth in shear flow exhibits universality. *Phys. Fluids A* **5**, 2298–2300.

Forster, G. K. & Craik, A. D. D. 1996 The stability of three-dimensional time-periodic flows with ellipsoidal stream surfaces. *J. Fluid Mech.* **324**, 379–391.

Hochstadt, H. 1975 *Differential Equations.* Dover.

Howard, L. N. 1961 Note on a paper of John W. Miles. *J. Fluid Mech.* **13**, 158–160.

Lavelle, J. W. & Smith, D. C. 1996 Effects of rotation on convective plumes from line segment source. *J. Phys. Oceanogr.* **26**, 863–872.

Lifschitz, A. & Hameiri, E. 1991 Local stability conditions in fluid dynamics. *Phys. Fluids* A **3**, 2644–2651.

Lilly, D. K. 1967 The representation of small-scale turbulence in numerical simulation experiments. In *Proc. IBM Scientific Computing Symp. on Environmental Science*, pp. 195–210.

Lombard, P. N. & Riley, J. J. 1996 On the breakdown into turbulence of propagating internal waves. *Dyn. Atmos. Oceans* **23**, 345–355.

https://doi.org/10.1017/S0022112098003085 Published online by Cambridge University Press

Majda, A. J. & Shefter M. G. 1998 The instability of stratified flows at large Richardson numbers. *Proc. Natl Acad. Sci. USA* **95**, 7850–7853.

Miles, J. W. 1961 On the stability of heterogeneous shear flows. *J. Fluid Mech.* **10**, 496–508.

Press, W. H., Teukolsky, S. A., Vetterling, W. T. & Flannery, B. P. 1992 *Numerical Recipes,* 2nd edn. Cambridge University Press.

Siegel, D. A. & Domaradzki, J. A. 1994 Large-Eddy simulation of decaying stably stratified turbulence. *J. Phys. Oceanogr.* **24**, 2353–2385.

Smagorinsky, J. 1963 General circulation experiments with the primitive equations. I. The basic experiment. *Mon. Weath. Rev.* **91**, 99–164.

Tabor, M. 1989 *Chaos and Integrability in Nonlinear Dynamics. An Introduction.* John Wiley & Sons.

https://doi.org/10.1017/S0022112098003085 Published online by Cambridge University Press